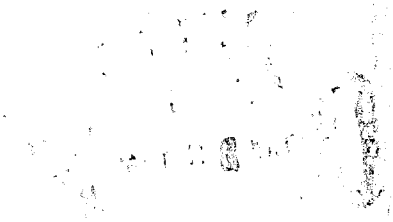

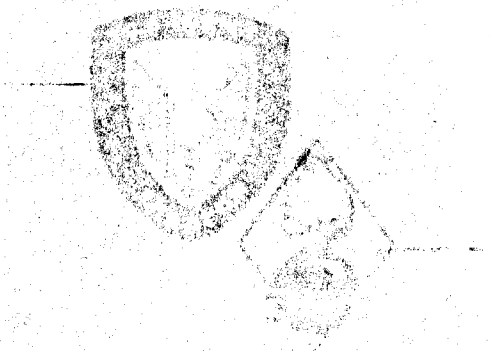

U.S. Army Electronics Research
and Development Command
Harry Diamond Laboratories

DISTRIBUTION OF THIS DOCUMENT IS UNLIMITED.

The findings in this report are not to be construed as an official Department of the Army position unless so designated by other authorized documents.

Citation of trade names in this report does not constitute an official indorsement or approval of the use of such items.

Destroy this report when no longer needed. Do not return it to the originator.

UNCLASSIFIED

SECURITY CLASSIFICATION OF THIS PAGE (When Data Entered)

REPORT DOCUMENTATION PAGE		READ INSTRUCTIONS BEFORE COMPLETING FORM
1. REPORT NUMBER HDL-TR-1985	2. GOVT ACCESSION NO. AD-A114713	3. RECIPIENT'S CATALOG NUMBER
4. TITLE (and Subtitle) Charge Generation and Recombination in Silicon Dioxide from Heavy Charged Particles		5. TYPE OF REPORT & PERIOD COVERED Technical Report 6. PERFORMING ORG. REPORT NUMBER
7. AUTHOR(s) Timothy R. Oldham		8. CONTRACT OR GRANT NUMBER(s) PRON: WJ1 7101WJA9 MIPR: 81-575
9. PERFORMING ORGANIZATION NAME AND ADDRESS Harry Diamond Laboratories 2800 Powder Mill Road Adelphi, MD 20783		10. PROGRAM ELEMENT, PROJECT, TASK AREA & WORK UNIT NUMBERS Program Ele: 6.27.15.H
11. CONTROLLING OFFICE NAME AND ADDRESS Director Defense Nuclear Agency Washington, DC 20305 and Director Defense Advanced Research Projects Agency Arlington, VA 22209		12. REPORT DATE April 1982 13. NUMBER OF PAGES 78 15. SECURITY CLASS. (of this report) UNCLASSIFIED 15a. DECLASSIFICATION/DOWNGRADING SCHEDULE

16. DISTRIBUTION STATEMENT (of this Report)

Approved for public release; distribution unlimited.

17. DISTRIBUTION STATEMENT (of the abstract entered in Block 20, if different from Report)

18. SUPPLEMENTARY NOTES HDL Project: 233123

This work was sponsored by the Defense Advanced Research Projects Agency and the Defense Nuclear Agency under DNA subtask M99QAXZB, work unit 00001, "Single Particle Physics."

19. KEY WORDS (Continue on reverse side if necessary and identify by block number)

Ionization	Silicon dioxide
SiO_2	Charge recombination
Single particle	Very large scale integrated circuit
Microelectronics	VLSIC

20. ABSTRACT (Continue on reverse side if necessary and identify by block number)

Metal-oxide-semiconductor (MOS) microelectronic circuits have long been known to be sensitive to gamma radiation, which causes ionization in the oxide film. In recent years, as the circuits have been reduced more and more in size, they have also been shown to suffer temporary upsets caused by single heavy charged particles in the natural environment. The purpose of this study was to determine the amount of ionization from a heavy charged particle that would escape recombination in a thin

DD FORM 1 JAN 73 1473 EDITION OF 1 NOV 65 IS OBSOLETE

UNCLASSIFIED

SECURITY CLASSIFICATION OF THIS PAGE (When Data Entered)

Item 20. ABSTRACT (Cont'd)

SiO_2 film. The implications of these findings for the operation of future microelectronic circuits are discussed briefly.

The MOS capacitors were irradiated with 2-MeV α particles or with 700-keV protons. The flatband voltage shift was determined by using the well-known capacitance-voltage (C-V) technique. This voltage shift is proportional to the amount of ionization that escapes recombination in the SiO_2.

The experimental results agree very well with a modified version of the columnar recombination model first proposed by George Jaffé in 1913. Jaffé developed an approximate analytical solution that is not entirely satisfactory. However, by using a large digital computer, one can solve Jaffé's exact differential equation numerically. If the column radius, b, is taken to be 3.5 nm, the results of a finite difference calculation fit the experimental results very well. At fields of 2 MV/cm, the yield of charge is about 10 percent for incident α particles and about 25 percent for protons.

These results are much less than the yield that one would expect for other forms of radiation. For this reason, one can probably conclude that electronic devices will probably not fail from single particle induced ionization until the devices are much smaller than those now on the drawing boards.

CONTENTS

FIGURES

FIGURES (Cont'd)

Page

FIGURES (Cont'd)

Page

FIGURES (Cont'd)

Page

TABLES

1. INTRODUCTION

In recent years, the effect of α particles and other ions passing through semiconductors has been a subject of intense interest. In 1978, May and Woods[1]* showed that so-called soft errors or upsets in microelectronic circuits were sometimes caused by α particles from radioactive contaminants in the ceramic packaging around the circuit. When such a particle passes through a silicon (Si) chip, it generates a large number of electron-hole pairs. Sometimes enough charge is collected to upset a memory element (that is, to change its state). Since this effect was identified, several other investigators[2-5] have studied the effects of other kinds of cosmic rays and other charged particles in semiconductors.

In this study, we consider the effects of heavy charged particles in insulating silicon dioxide (SiO_2) films rather than in semiconductors. Amorphous SiO_2 is an insulator of great fundamental interest because it has a high dielectric strength and its electronic properties have been studied at fields an order of magnitude or more higher than most other insulators.[6] Thermally grown SiO_2 is also a material of great practical interest because of its role in metal-oxide-semiconductor (MOS) microelectronic circuits and in integrated optics. It has long been known that SiO_2 is extremely sensitive to ionizing radiation, and its response to electron beam and gamma radiation has been studied extensively. References 7 to 11 are a representative but far from complete bibliography. Thus, there are fundamental reasons as well as practical reasons to study the effects of heavy charged particles in thin films of amorphous SiO_2.

In the work reported here, we conducted a series of experiments in which MOS capacitors were exposed to a beam of ions, and the fraction of charge escaping recombination was determined. Then we adapted the Jaffé columnar recombination model to fit a curve to the experimental results with reasonably good agreement. The model can be used to calculate the recombination for particles and energies different from those used in the experiments. Both the experiments and the model are discussed in detail in this report.

2. HISTORICAL BACKGROUND

The problem of ionization of insulators by radiation is among the oldest in modern physics. The theory of ionization and recombination in gases was first based on the assumption of uniform ionization throughout the total volume of the gas. Bragg and Kleeman[12,13] were the first to show that for α particle irradiation, the recombination is much stronger than can be explained by a theory based on uniform ionization. They

*See references in Literature Cited section.

both tried to explain their results in terms of an "initial recombination" model (also now called geminate recombination), which assumed that ions in a pair originating from the same molecule have a strong special tendency to recombine with each other. This geminate recombination model has been further developed by Smoluchowski,[14] Onsager,[15] and others,[16-19] and it has proved useful in treating many problems, although some problems seem to require more complicated analysis.[20-23] However, Moulin[24,25] showed that it did not apply to α particles in gases.

Langevin[26,27] was the first to realize that the ionization produced by α particles was in extremely dense columns about the particle track so that the recombination would be much stronger than predicted by a theory based on uniform ionization. Langevin argued that the recombination was governed by the following equation:

$$\frac{\partial n_{\pm}}{\partial t} = -\alpha n_{+} n_{-} \quad , \tag{1}$$

where $n_{\pm}$ is the density of positive (or negative) charge. He also obtained an analytical expression for the recombination coefficient α. The results obtained by Moulin were consistent with the Langevin hypothesis.

The Langevin theory was refined by Jaffé in a classic paper in 1913.[28] Jaffé added a diffusion term to account for random thermal motion and a drift term to account for the effect of a constant external field to the Langevin equation (1). Thus, the evolution of the columns of charge produced by an α particle is described by the following differential equation:

$$\frac{\partial n_{\pm}}{\partial t} = D_{\pm} \nabla^2 n_{\pm} \mp \mu_{\pm} E \frac{\partial n_{\pm}}{\partial x} - \alpha n_{+} n_{-} \quad , \tag{2}$$

where the α particle travels along the z-axis, D is the diffusion coefficient, μ is the mobility of the charged particles, and E is the component of the field in the x-direction. D and μ may be different for the positive and negative species. Jaffé was not able to solve this equation exactly, so he neglected the recombination term and solved the rest of the equation, getting the standard diffusion result. Then he reintroduced the effect of the recombination term by letting the total number of charges, N, vary with time, t. By this procedure, he obtained the following approximate expression for the amount of charge escaping recombination:

$$Y = \left[1 + \left(\frac{\pi}{2}\right)^{1/2} \frac{N_0 e}{4\pi\varepsilon\varepsilon_0 bE \sin\theta}\right]^{-1} \quad , \tag{3}$$

where

Y is the yield of charge (fraction escaping recombination),
N_0 is the total number of ion pairs per centimeter,
e is the electron charge,
ε is the relative dielectric constant of the medium,
ε_0 is the permittivity of free space,
b is the effective column radius,
E is the total applied field,
θ is the angle between the field and the particle track.

Since N_0 and b were not known in 1913, Jaffé treated them as adjustable parameters, and he was able to obtain good fits of equation (3) to his original experiments and also to a later series of experiments.[29,30]

Jaffé did most of his experiments with gases, although he also worked briefly with organic liquids. Gerritsen[31,32] did a series of experiments with α particles passing through liquified gases, and he obtained results that did not agree very well with Jaffé's approximate solution (eq 3). In an effort to explain Gerritsen's results, Kramers[33] developed a different approximate solution to Jaffé's differential equation (eq 2). Kramers neglected the diffusion term and obtained an analytical solution to the remaining equation. Then he attempted to reintroduce the effect of the diffusion term. This procedure was not very satisfying since the diffusion correction is unphysical, and the agreement between Kramers' theory and Gerritsen's experiments also was not as good as one could wish.

One can see from the preceding discussion that the ionization produced by α particles passing through matter is an old problem that has been studied extensively. A great deal has been learned, but significant questions remain even for materials that were studied in the past. For a fundamentally different material such as thermally grown SiO_2, very little is known with certainty until experiments are performed.

3. EXPERIMENTAL PROCEDURE AND RESULTS

In our experiments, we used dry oxide MOS capacitors on n-type Si prepared by Hughes Aircraft Corp. The samples had an oxide thickness of 135 nm and an electrode area of 0.0032 cm^2 (0.025-in. diameter). The electrodes were thin aluminum (105 nm thick) with bonding pads on the edge for electrical contact. The samples were mounted on TO-5 headers, and electrical contact was made by thermocompression gold wire bond.

The samples were irradiated under positive bias at approximately liquid nitrogen temperature (~77 K). The samples were mounted in a

copper (Cu) cold finger, which was in contact with a liquid nitrogen reservoir. The temperature was monitored with a Cu-constantan thermocouple.

When an ion or any ionizing radiation passes through the SiO_2 film, it loses energy by creating electron-hole pairs. At liquid nitrogen temperature, the electrons are swept out of the SiO_2 almost instantaneously, but the holes have only a negligible mobility. For example, Hughes has shown[10] that the electrons have a mobility of 20 $cm^2/V\text{-}s$ at room temperature and 40 $cm^2/V\text{-}s$ extrapolated to liquid nitrogen temperature. Thus, for fields on the order of 10^6 V/cm and an SiO_2 thickness on the order of 10^{-5} cm, all the electrons are swept out of the SiO_2 in less than 1 ps both at room temperature and at 77 K.

The holes, on the other hand, have a much lower mobility, and they do not move by a conventional "drift" process. The holes move by a dispersive hopping process, which has been extensively studied[7,34,35] and which has been shown to be both temperature dependent[36] and field dependent.[37] At liquid nitrogen temperature, the mobility of the holes is 10^{-11} $cm^2/V\text{-}s$ or less, depending on the applied field. It has been shown[8] that hole transport is negligible at times of 100 s or even more at applied fields of 2 MV/cm or less. At an applied field of 3 MV/cm, the transport is not a large effect, but it is detectable. Thus, the electrons are removed from the SiO_2 "instantaneously," and the holes are frozen in place for times long compared with the experimental times. At room temperature, on the other hand, significant hole transport would occur during the experiment, and the results would be difficult to interpret.

The α particle and proton irradiations were carried out at the Naval Surface Weapons Center (NSWC) Van de Graaff facility. The α particles had a kinetic energy of 2 MeV, and the protons had a kinetic energy of 700 keV. In both irradiations, the beam was brought into the test chamber and scattered by a 200-nm Cu foil. The particle flux was determined by using two surface barrier detectors: one was in the sample position (about 6 deg above the beam axis), and the second (monitor) detector was off at a large angle (>45 deg) from the beam axis (fig. 1). The ratio of counts in the two detectors was nearly constant in a series of calibration exposures (table 1).

In principle, the ratio of counts in the two detectors could be calculated from the Rutherford cross section if the angle were measured precisely. But if the sample were raised 0.05 in. (1.27 mm), that is, if the angle were increased less than 0.5 deg, the ratio of counts in the two detectors would be reduced approximately 30 percent. Since our test capacitors were located anywhere on a TO-5 header, that is, not necessarily centered, we could get large variations in particle count at the sample for a constant particle count at the monitor detector. Few

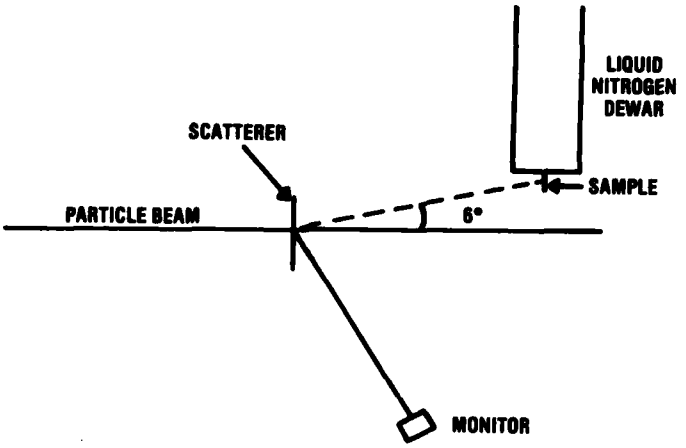

Figure 1. Experimental schematic for α particle and proton exposures.

TABLE 1. RESULTS OF CALIBRATION EXPOSURES OF α PARTICLES AND PROTONS

Calibration	Exposure	Sample position	Monitor detector	Exposure (s)
Initial, helium ions, 1-mm aperture	1	911769	11032	138.2
	2	856319	10023	90.4
	3	858821	9985	49.5
	4	850685	10017	50.2
	5	858404	10022	80.2
Sample raised 1.27 mm	1	607824	9995	51.6
	2	606287	9988	53.7
	3	598782	10028	51.9
	4	594426	10027	51.2
	5	593954	10025	52.8
Proton, 1-mm aperture	1	501689	10063	-
	2	503328	10050	-
	3	497349	10051	-
	4	503061	10073	-
	5	510102	10074	-

things in nuclear physics are as well established as the Rutherford cross section, but it varies so strongly with position at small angles that we could not rely on it to determine the incident particle count at the sample.

The method finally settled on for counting incident particles was to use the sample as its own detector. After the sample had been exposed at positive bias and the flatband voltage shift (ΔV_{FB}) had been determined, the bias was reversed so that the sample was in depletion. The MOS capacitor was then used like a surface barrier detector with the depletion region in the Si being the sensitive volume. Then the exposure was repeated, and the current pulses in the capacitor were counted by a multichannel spectrum analyzer.

Figure 2 is a schematic diagram of a sample during the particle counting. As an α particle passes through an MOS capacitor, it creates electron-hole pairs in the SiO_2 and in the Si substrate. The dashed line represents the depth in the Si of the depletion layer. The free charge in the depletion layer appears as a current pulse, which is counted by the spectrum analyzer. A typical spectrum is shown in figure 3. A background measurement indicated that the low-energy counts (below the marker) were present with the beam blocked off, but only about 1000 counts above the mark were noise.

The aluminum gate electrodes are thin enough that the energy lost by the charged particles is almost negligible. A 2-MeV α particle passing through 105 nm of aluminum (Al) loses slightly less than 0.04 MeV.[38] For the protons, the energy lost in the gate electrode is even less, 0.005 MeV. Thus, a known number of particles of known energy were incident on the SiO_2 film. The amount of charge created could then be calculated very accurately. The amount of charge that escaped recombination was determined by measuring the ΔV_{FB} using the well-known capacitance-voltage (C-V) technique.[39] Typical C-V curves are shown in figure 4. The irradiation took place at 77 K, and the preirradiation and postirradiation C-V traces were recorded. The average fluence of α particles and protons on the sample was $1.6 \times 10^8/cm^2$ and $1.06 \times 10^8/cm^2$, respectively. For the very thin SiO_2 (135 nm), the energy loss per unit path length was uniform across the SiO_2 for these high energy particles. The calculated total dose in the SiO_2 was 3.8 krad (SiO_2) from the α particles and 0.54 krad (SiO_2) from the protons.

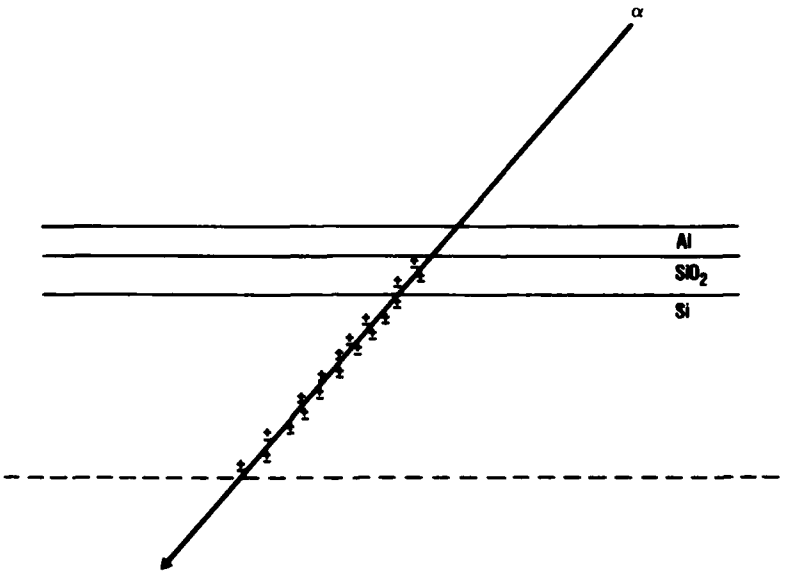

Figure 2. Sample schematic showing metal, SiO_2, and depletion region of Si substrate.

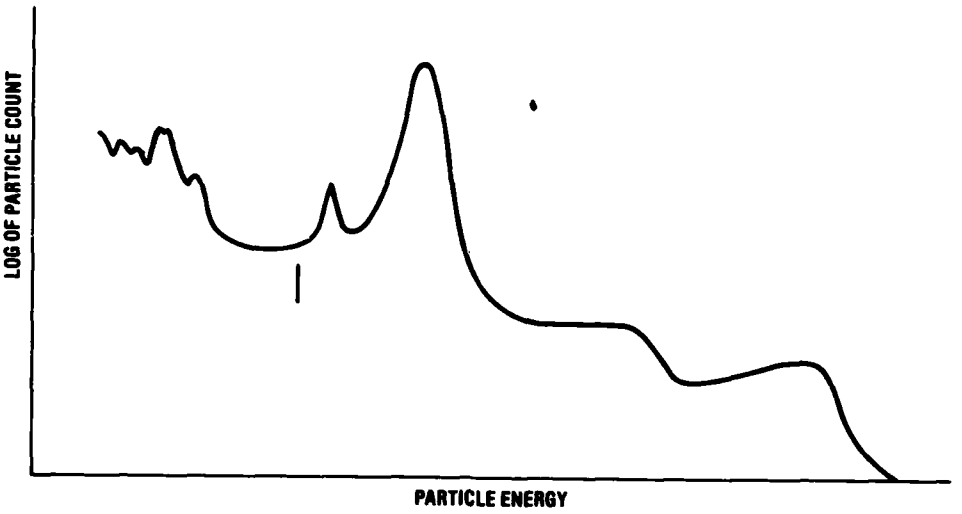

Figure 3. Typical α particle spectrum as recorded by metal-oxide-semiconductor capacitor; logarithm of particle count is plotted against particle energy; low-energy noise (below mark) is subtracted out.

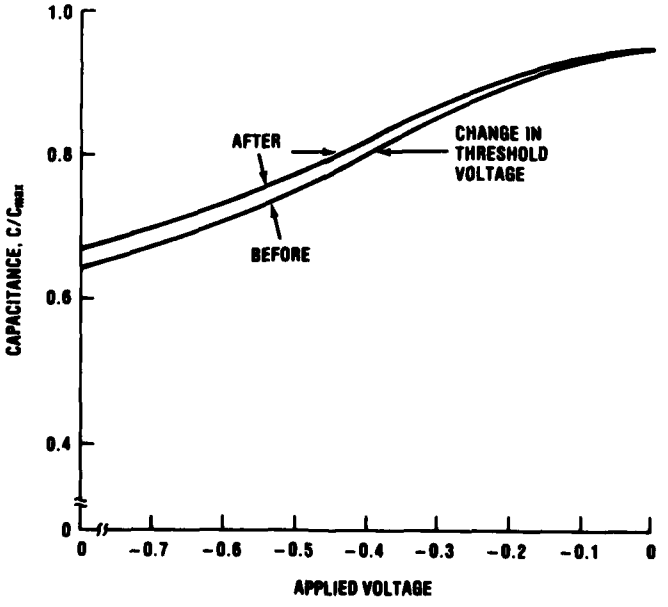

Figure 4. Typical capacitance-voltage curve from this experiment.

The total ΔV_{FB} was assumed to be proportional to the average yield of holes that escaped recombination and were immobilized in the SiO_2. The ΔV_{FB} is proportional to the first moment of the charge distributions, and in this case the holes are created and frozen in place uniformly across the SiO_2. Under these conditions,

$$\Delta V_{FB} = \frac{1}{C_{ox}} \int_0^{\ell_{ox}} \rho(x) \frac{x}{\ell_{ox}} dx \qquad (4)$$

reduces to

$$\Delta V_{FB} = \frac{1}{2} \frac{Q}{C_{ox}} \quad , \qquad (5)$$

where

C_{ox} = oxide capacitance, $\varepsilon\varepsilon_0/\ell_{ox}$,

ε = 3.85 for SiO_2,

$\varepsilon_0 = 8.85 \times 10^{-14}$ f/cm,

ℓ_{ox} = oxide thickness,

Q = charge, $f(E)Q_0$,

$f(E)$ = experimentally determined fractional yield of charge surviving recombination,

Q_0 = total amount of positive charge generated by irradiation,

$$Q_0 = \left|\frac{dT}{dx}\right| \frac{\ell_{ox}}{\cos\theta} \frac{1.6 \times 10^{-19} \text{ coulomb/hole}}{18 \text{ eV}} \quad , \qquad (6)$$

where

dT/dx = energy loss per unit path length,

18 eV = electron-hole pair creation energy that has been reported.[40-43]

The procedure was to measure the ΔV_{FB} as a function of the applied field. The fractional yield was then determined by dividing the measured $\Delta V_{FB}(E)$ by the calculated maximum ΔV_{FB}, assuming no recombination.

Since one would expect the charge yield to depend on the angle between the field and the particle beam, we performed three series of measurements: (1) with α particles incident at 45 deg; (2) with α particles as close as possible to normal incidence, 6 deg; and (3) with protons incident at 45 deg (tables 2 to 4; fig. 5 and 6).

TABLE 2. HELIUM ION RESULTS AT 45 DEG

Shot	Sample	Applied field (MV/cm)	Change in threshold voltage (V)	α particle count	Monitor count	Fractional yield
1	118	1.48	0.106	499062	25100	0.087
2	159	1.11	0.069	423646	25534	0.066
3	104	0.89	0.051	363908	25025	0.058
4	153	0.37	0.031	355028	24993	0.036
5	125	0.22	0.026	339447	25108	0.031
6	160	0.15	0.028	469308	25041	0.024
7	137	0.07	0.015	393174	25000	0.016
8	129	0	0.020	410312	25041	0.014
9	112	0.37	0.033	370939	25081	0.036
10	30	0.52	0.045	349000	24822	0.055
11	130	0.74	0.047	349000	24822	0.055
12	152	2.22	0.055	182605	25049	0.113
13	135	1.85	0.098	418907	25052	0.096

TABLE 3. HELIUM ION RESULTS AT 6 DEG

Shot	Sample	Applied field (MV/cm)	Change in threshold voltage (V)	α particle count	Monitor count	Fractional yield
1	132	1.48	0.083	735248	25074	0.065
2	146	0.74	0.051	684609	25055	0.041
3	113	0.37	0.024	589315	25034	0.024
4	161	1.11	0.057	499087	25062	0.050
5	102	1.85	0.094	498744	25126	0.077
6	96	2.22	0.102	644746	25083	0.091
7	126	2.59	0.071	520040	25072	0.095
8	101	2.96	0.114	666302	25084	0.098
9	140	0.15	0.029	574529	25033	0.020

TABLE 4. PROTON RESULTS AT 45 DEG

Shot	Sample	Applied field (MV/cm)	Change in threshold voltage (V)	Particle count	Monitor count	Fractional yield
1	20	1.48	0.035	356659	25054	0.310
2	104	0.74	0.026	389967	25079	0.211
3	138	1.11	0.037	373653	25088	0.290
4	51	0.37	0.039	742379	25059	0.147
5	16	0.15	0.016	380000	25079	0.113
6	54	2.22	0.038	289219	25069	0.374
7	142	1.85	0.039	312000	25116	0.351
8	156	2.96	0.057	342204	25077	0.465
9	44	2.59	0.043	270247	25051	0.439

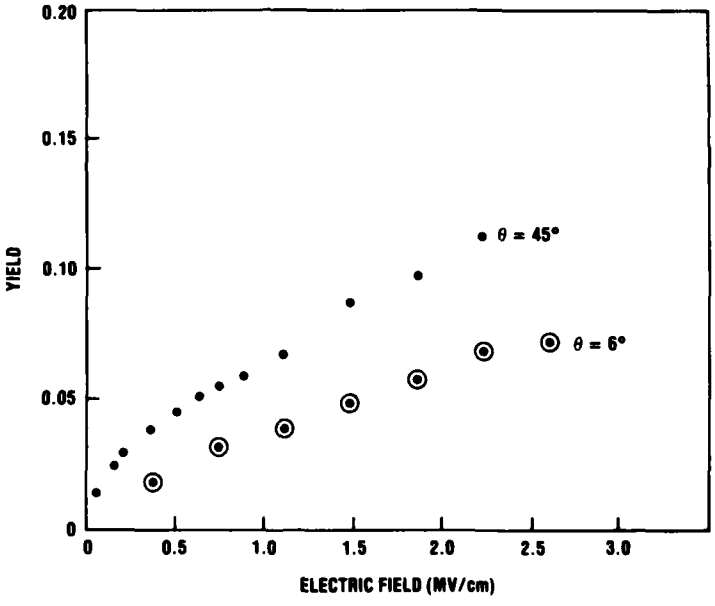

Figure 5. Experimental results for α particles incident at 45 and 6 deg between field and particle track (θ).

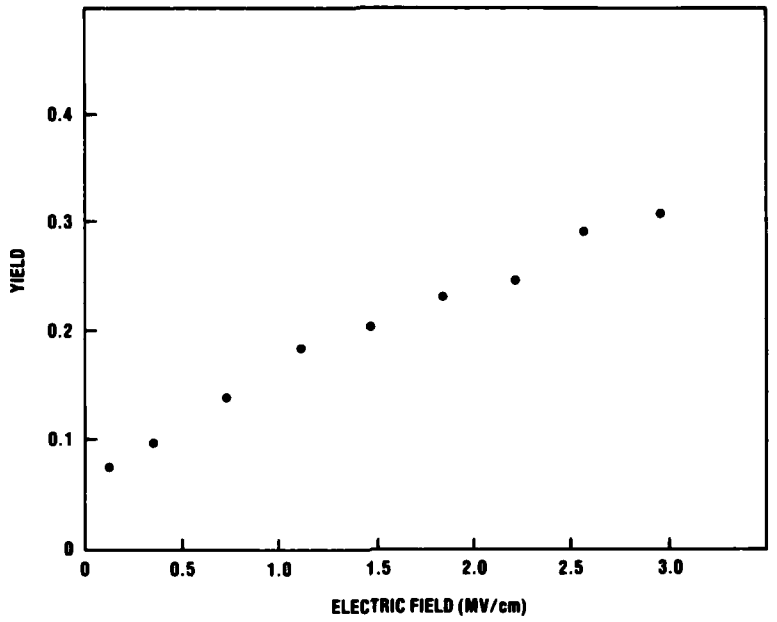

Figure 6. Experimental results for protons incident at 45 deg.

One can see from figures 5 and 6 that the fraction of charge escaping recombination is only a small fraction of the total charge generated by a highly ionizing particle. For comparison, we show in figure 7 the results of these experiments along with previously published results for electrons.[39,40] For high-energy electrons, the yield is close to 100 percent at fields above ~2 MV/cm; but for α particles the yield is on the order of 10 percent at 2 MV/cm, and for protons the yield is ~25 percent at 2 MV/cm. The results in figure 7 show dramatically the effect of recombination along the track of a heavy ion.

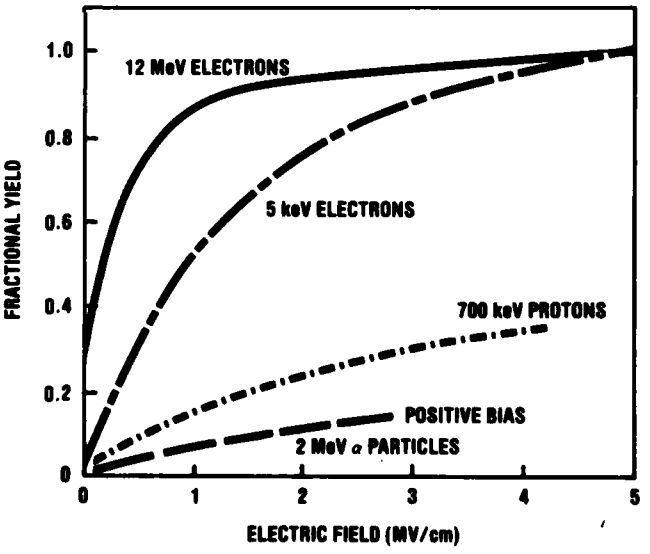

Figure 7. Comparison of α particle and proton results with previously published results for electrons.

4. ANALYSIS

This section discusses the physical model that describes the experimental results. In particular, we detail the Jaffé model[28] as originally developed and as applied here.

Jaffé began by assuming that the charge distribution produced by an α particle is uniform along the z-axis, that is, along the particle track. The initial density of free charge about the axis is assumed to be Gaussian and given by

$$n_{\pm}(r,o) = \frac{N_0}{\pi b^2} e^{-r^2/b^2} \quad , \tag{7}$$

where N_0 is the total number of electron-hole pairs produced per unit path length and b is the column radius.

Then Jaffé treated the case in which no external field is present and the evolution of the charge distributions is given by

$$\frac{\partial n_{\pm}}{\partial t} = D\nabla^2 n_{\pm} - \alpha n_{+} n_{-} \quad , \tag{8}$$

where the first term on the right is the diffusion term and the second term is the recombination term. Jaffé chose to develop an approximate solution to equation (8) by neglecting the recombination term and solving the diffusion equation first. He obtained the standard result

$$n_{\pm}(\vec{r},t) = \frac{N_0}{\pi(4Dt + b^2)} e^{-r^2/(4Dt+b^2)} \quad . \tag{9}$$

Then he allowed for the effect of recombination by replacing N_0 with N(t) in equation (9) and substituting equation (9) into equation (8). The result was an expression for dN(t)/dt, which could be integrated to obtain the result

$$N(t) = \frac{N_0}{1 + \frac{\alpha N_0}{8\pi D} \ln \frac{4Dt + b^2}{b^2}} \tag{10}$$

or

$$n_{\pm}(n,t) = \frac{N_0}{1 + \frac{\alpha N_0}{8\pi D} \ln \frac{4Dt + b^2}{b^2}} \; \frac{e^{-r^2/(4Dt+b^2)}}{\pi(4Dt + b^2)} \quad . \tag{11}$$

Next, Jaffé calculated the fraction of charge diffusing outside a radius, R (comparable to the separation between columns), which was considered to have escaped recombination at any time, t. This calculation was performed by integrating equation (11) over space and time with the fraction of charge surviving at infinite time,

$$\frac{N_1}{N_0} = -\int_{\xi_0}^{0} \frac{e^{-\xi}\, d\xi}{1 + \frac{\alpha N_0}{8\pi D} \ln \frac{\xi_0}{\xi}} \quad , \tag{12}$$

where

$$\xi = \frac{R^2}{4Dt + b^2} \, ,$$

$$\xi_0 = \frac{R^2}{b^2} \, ,$$

$$d\xi = \frac{-4DR^2}{(4Dt + b^2)^2}\, dt \, .$$

Since R is generally large compared with b, it is sufficient to evaluate the integrand at the upper limit, $t \to \infty$. The integrand in equation (12) is plotted in figure 8, and the integral can be evaluated numerically. The yield for 2-MeV α particles in SiO_2 is less than 1 part in 10^3.

The zero field case corresponds to two cylinders of charge, one positive and one negative, spreading out under the influence of diffusion and undergoing recombination at the same time. Next, Jaffé considered these same cylinders in the presence of an external electric field. The basic assumptions here are that (1) the charge densities are sufficiently small that the electron-hole interactions are small compared with interactions with the field, that is, $e^2/\langle r^{ij} \rangle \ll eE\lambda$, and (2) screening is negligible ($b < \lambda_{Debye}$). The first of those conditions is not really satisfied until considerable recombination has taken place, so one would expect the theory to make reasonable predictions only at late time.

First, Jaffé considered the case where the field is parallel to the column axis and the cylinders move as indicated schematically in figure 9. If field E is applied between the plates of a capacitor with separation L, then the time for the cylinders to move past each other is given by $T = L/2\mu E$. (2μ is replaced by $\mu_+ + \mu_-$ if the positive and negative charges have different mobilities.) The region where the cylinders overlap is described by the zero field calculation stated

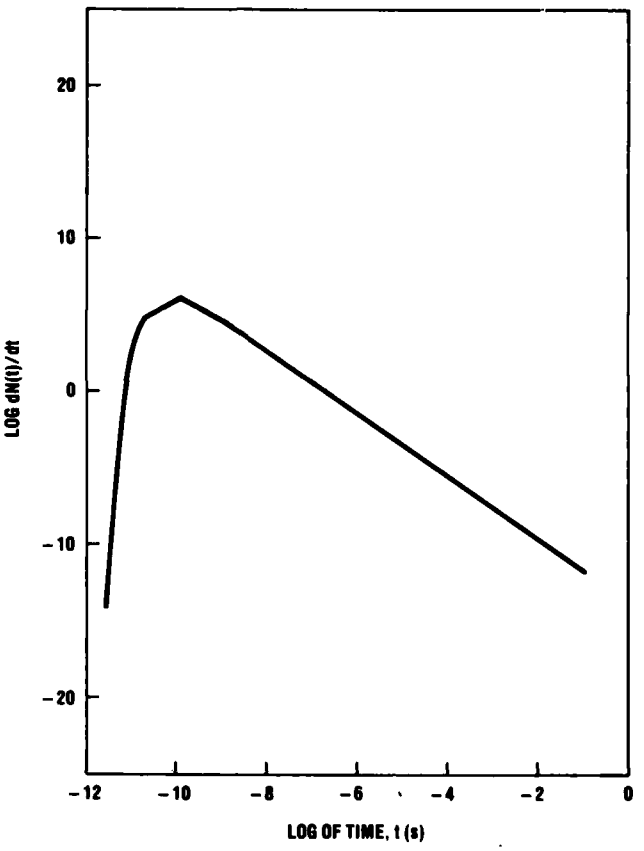

Figure 8. Jaffé's calculation for rate at which ions escape recombination in absence of applied field for SiO_2 (yield = 1.49×10^{-4}).

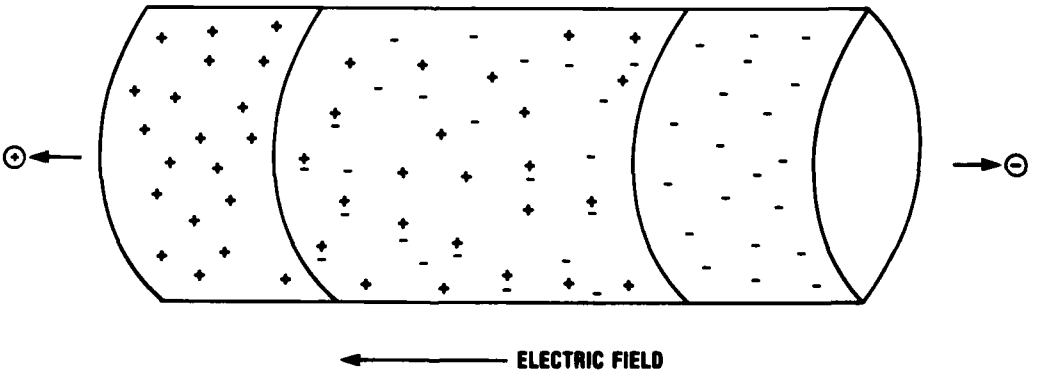

Figure 9. Schematic of two cylinders of charge moving past each other as in Jaffé's calculation for field parallel to particle track.

above, but no further recombination takes place in the parts of the cylinders where the positive and negative distributions no longer overlap. The number of charges of each sign that escape from the volume of overlap in time increment dt is $2\mu EN(t)\,dt$, and the total number of free charges that escape recombination is given by

$$N_2 = 2\mu E N_0 \int_0^T \frac{dt}{1 + \frac{\alpha N_0}{8\pi D} \ln \frac{4Dt + b^2}{b^2}} \quad . \tag{13}$$

Using the logarithmic integral,

$$\mathrm{li}(x) = \int_0^x \frac{dt}{\ln t} \quad ,$$

tabulated by Jahnke and Emde,[44] one can compute the fractional yield, $Y = N_2/N_0 L$, which can be shown to be

$$Y = \frac{\mu}{2D} E \frac{b^2}{L} y_1 e^{-y_1} \left(\mathrm{li}\, e^{y_2} - \mathrm{li}\, e^{y_1}\right) \quad , \tag{14}$$

where

$$y_1 = \frac{8\pi D}{N_0 \alpha} \, ,$$

$$y_2 = \frac{8\pi D}{\alpha N_0} + \ln \frac{4DT + b^2}{b^2} \quad .$$

Evaluating equation (14) for SiO_2 leads to the results plotted in figure 10 for two values of L.

Second, Jaffé considered the case where the field is perpendicular to the particle track as indicated schematically in figure 11. He solved the following differential equation by first neglecting the recombination term:

$$\frac{\partial n_\pm}{\partial t} = D_\pm \left(\frac{\partial^2 n_\pm}{\partial x} + \frac{\partial^2 n_\pm}{\partial y^2} \right) \mp \mu_\pm E \frac{\partial n_\pm}{\partial x} - \alpha n_+ n_- \quad . \tag{15}$$

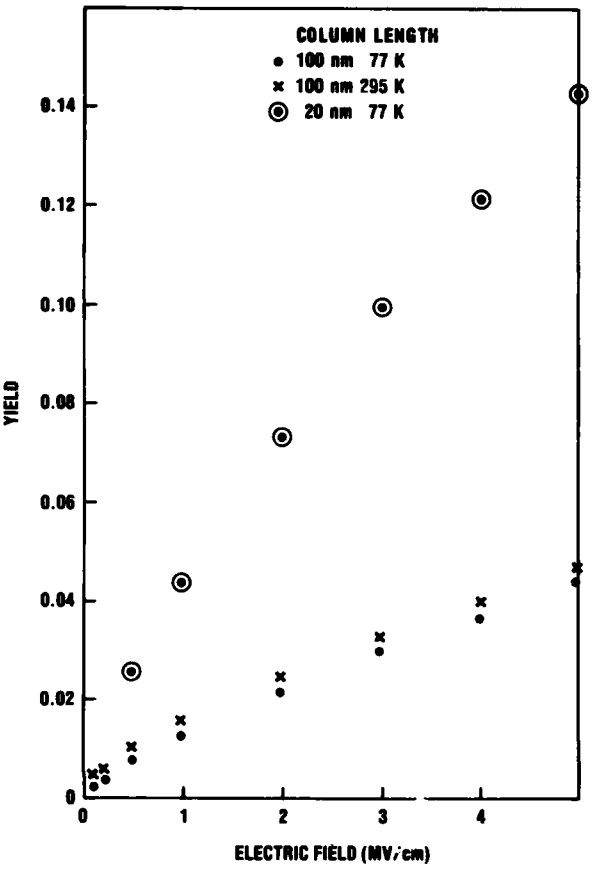

Figure 10.

Yield calculated for normally incident α particle using Jaffé's procedure for SiO_2.

The particle track is here taken to be along the z-axis, and the field is taken to be along the x-axis. When this equation is solved without the recombination term, one obtains the result

$$n_{\pm} = \frac{N}{\pi(4Dt + b^2)} \exp\left[-\frac{(x \mp \mu Et)^2 + y^2}{4Dt + b^2}\right], \qquad (16)$$

where r^2 has been replaced with $x^2 + y^2$. Equation (16) is the standard diffusion result for two cylinders of charge spreading through diffusion and being pulled apart as shown in figure 12. Then Jaffé substituted equation (16) into equation (15), letting N be a function of t (only), and obtained the result

$$N(t') = \frac{N_0}{1 + \frac{\alpha N_0}{2\pi}\int_0^{t'} \frac{\exp\left(-\frac{2\mu^2 E^2 t^2}{4Dt + b^2}\right)}{4Dt + b^2}\, dt}. \qquad (17)$$

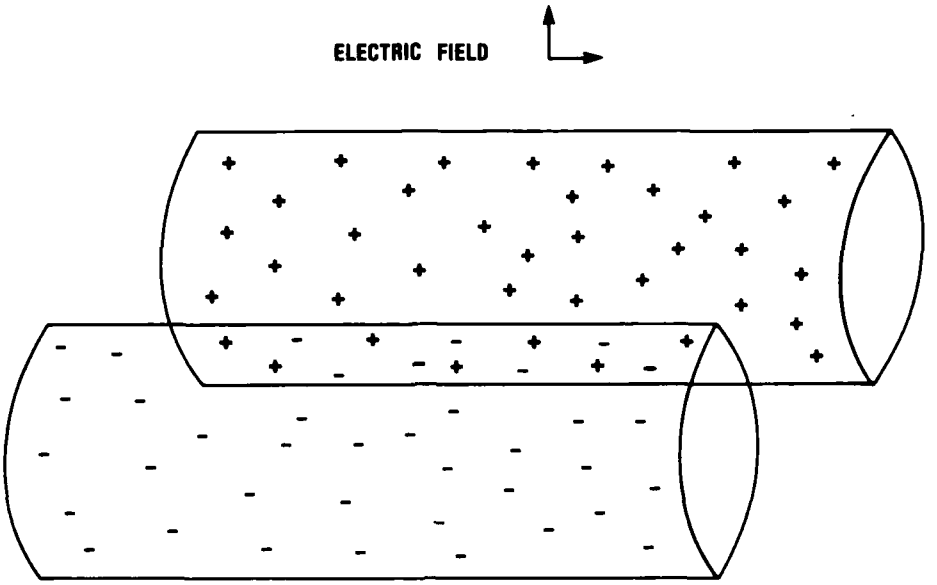

Figure 11. Schematic of two cylinders of charge moving under influence of normal field and parallel field (that is, arbitrary angle of incidence).

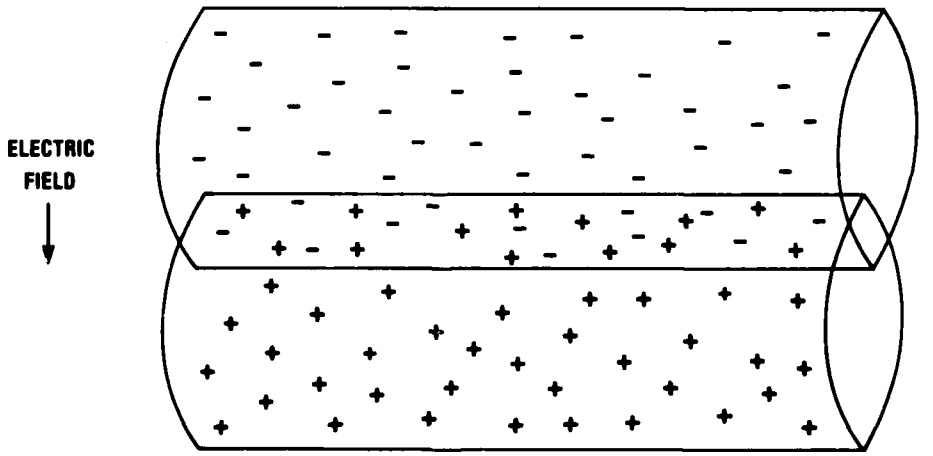

Figure 12. Schematic of two cylinders of charge moving under influence of normal field.

If equation (17) is substituted into equation (16), one obtains the approximate solution to equation (15). To get the yield of charge, one has to perform the integration in equation (17) from t = 0 to t = ∞, with the following result:

$$Y(E) = \frac{N_\infty}{N_0} = \frac{1}{1 + \frac{\alpha N_0}{8\pi D}\left(\frac{\pi}{z}\right)^{1/2} S(z)} \quad , \tag{18}$$

where

$$S(z) = \left(\frac{z}{\pi}\right)^{1/2} e^{z/2}\left(\frac{i\pi}{2}\right) H_0^{(1)}\left(\frac{iz}{2}\right) \quad , \tag{19}$$

$$z = \frac{b^2\mu^2E^2}{2D^2} \quad .$$

Here, $H_0^{(1)}$ is the Hankel function of the first kind.

Third, Jaffé treats the case of arbitrary angle between field and particle based on the two special cases already considered (fig. 13). If the angle between the field and the particle track is taken to be θ, then the time for the cylinders to move past each other is

$$T' = L/2\mu E \cos\theta \quad ,$$

which is analogous to the parallel field case. The number of charges escaping recombination is

$$N_3 = 2\mu E \cos\theta \int_0^{T'} N(t)\, dt$$

as before, where E has been replaced by the relevant component, E cos θ. The fractional yield is given by

$$Y(E) = \frac{N_3}{LN_0} = \frac{2\mu E \cos\theta}{L} \int_0^{T'} \frac{dt'}{1 + \frac{\alpha N_0}{2\pi} \int_0^{t'} \frac{\exp\left(-\frac{2\mu^2E^2 \sin^2\theta t^2}{4Dt + b^2}\right)}{4Dt + b^2}\, dt} \quad . \tag{20}$$

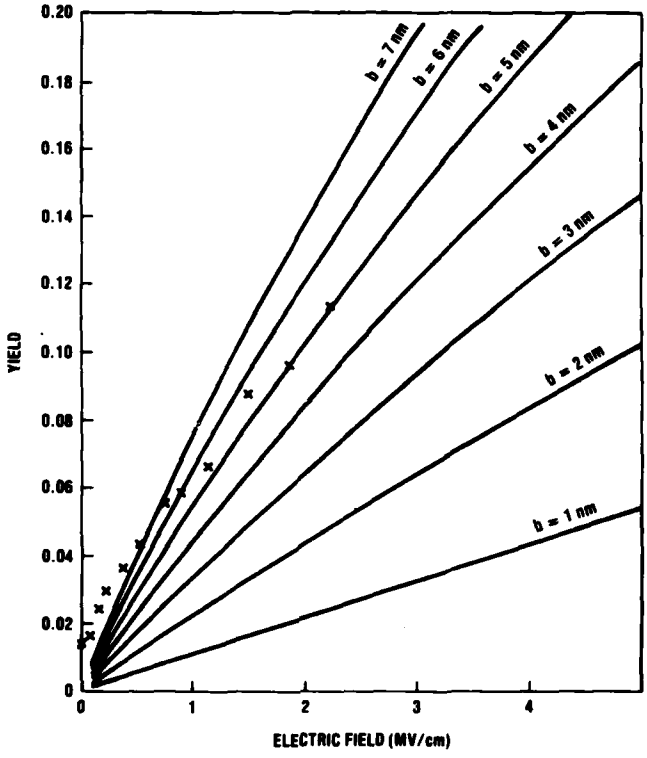

Figure 13. Experimental results for α particles at 45 deg compared with Jaffé's approximate solution, where column radius, b, is taken to be adjustable.

In equation (20), one can recognize equation (17) with field E replaced by the normal component, E sin θ. Equation (20) can be evaluated with the result

$$Y(E) \cong \frac{1}{1 + \frac{\alpha N_0}{8\pi D}\left(\frac{\pi}{z'}\right)^{1/2} S(z')} \quad , \tag{21}$$

where $z' = (b^2\mu^2E^2 \sin^2 \theta)/2D^2$. Equation (21) is only approximately equal to equation (20) because an end contribution has been neglected, but Jaffé argues that it is small in practice. For fields of practical interest in SiO_2 (that is, high fields), one can use the asymptotic expansion $iH_0^{(1)}(iz) \cong e^{-z}/(\pi x/2)^{1/2}$ and get

$$Y(E) = \left\{1 + \frac{\alpha N_0}{8\pi D}\left[\left(\frac{\pi}{2}\right)^{1/2} \frac{2D}{b\mu E \sin \theta}\right]\right\}^{-1} \quad . \tag{22}$$

The recombination coefficient α was determined by Langevin[26] to be

$$\alpha = \mu e/\varepsilon\varepsilon_0 \quad ,$$

and equation (22) becomes

$$Y(E) = \left[1 + \left(\frac{\pi}{2}\right)^{1/2} \frac{N_0 e}{4\pi\varepsilon\varepsilon_0 bE \sin\theta}\right]^{-1} \quad , \tag{23}$$

which is identical with equation (3). Jaffé was able to explain his experiments adequately with this model, treating both N_0 and b as adjustable parameters.[25-27] However, N_0 can be obtained independently by using the Bethe theory[45,46] or (recently) Ziegler's compilation,[38] so a modern researcher has only one free parameter, the column radius, in applying this model. In figure 13, we replot our experimental results for α particles along with the Jaffé solution for several values of b. One can see that the agreement between the Jaffé theory and the experiment is qualitative at best. The curves do not have the same shapes, but for a narrow range of E values one could pick a value of b that would give approximately the correct yield.

In measuring the yield of charge in liquified gases, Gerritsen encountered similar problems.[31,32] That is, the Jaffé model fitted his results only roughly. Kramers,[33] a colleague of Gerritsen, proposed a modification of the Jaffé treatment to try to explain Gerritsen's results. Kramers first neglected the diffusion term in equation (15) (or eq 2) and then by a complicated procedure obtained an analytical solution to the remaining equation. The result is plotted in figure 14 along with the Jaffé solution for comparison. In figure 14, the fractional yield is plotted as a function of reduced field, $f = F/F_o$, where F is the applied field and

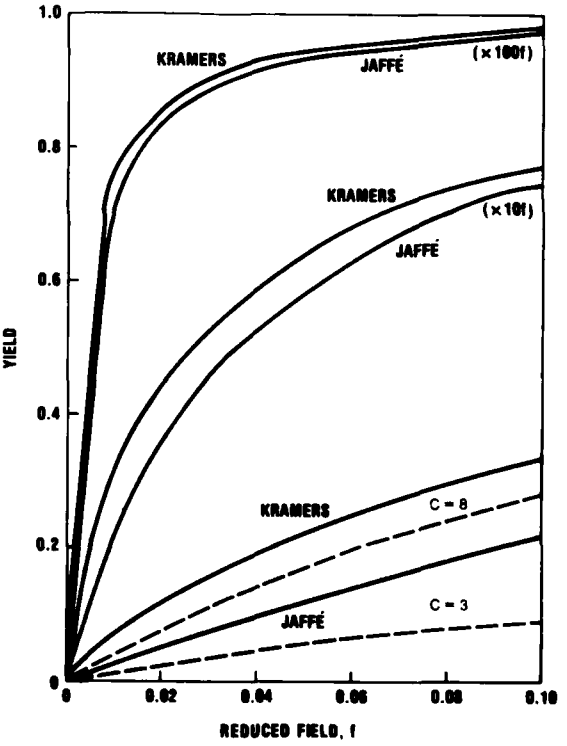

Figure 14. Kramers' approximate solution compared with Jaffé's expression.

F_o is a reference field. When Kramers reintroduced the effect of the diffusion term, he was left with an arbitrary integration constant, C, which has no physical meaning. The dashed lines in figure 14 are the fractional yield for two selected values of this constant C. One can see from figure 14 that the yield is rather sensitive to the value chosen for this parameter.

This situation is extremely unsatisfying. It is one thing to estimate a physical quantity such as the column radius, which is unknown but which can, in principle, be determined independently. It is another thing to pluck out of thin air a constant that has no meaning and that cannot be checked, but that nevertheless is critical. Thus, we do not use Kramers' result. But we should note in passing that even with the diffusion "fudge factor," the Kramers' theory did not fit Gerritsen's experiments well. In the end, Gerritsen had to assume that the column radius took on different values at high fields and at low fields to get reasonable agreement. This assumption is best greeted skeptically.

The value of Kramers' discussion is that he points out that, at least at low temperatures, the recombination term in equation (15) (or eq 2) is by far the largest term, with the drift term next and the diffusion term smallest. But rather than neglecting a term to simplify the analysis, one can use a large digital computer to solve the exact equation numerically. Today, even a pedestrian researcher can perform analysis unimaginable to either Jaffé or Kramers before the age of microelectronics.

The approach here is to use the initial Gaussian distribution postulated by Jaffé (eq 7) and to calculate the distribution of charges using a two-dimensional finite difference code and equation (15). The results can be generalized to three dimensions by a process similar to that used to get from equation (18) to equation (21).

The code written for this analysis calculates the initial density of charge at each point in a two-dimensional Cartesian grid with a maximum of 200 x-values and 100 y-values. The particle is assumed to travel along the z-axis, and the field is assumed to be along the x-axis. (Since the problem is symmetric in y, it serves no purpose to grind out the calculation in the lower half plane.) The grid spacing is variable in principle but, for all the calculations reported here, the points were 0.5 nm apart. Since the calculation is two dimensional, it describes only the region of overlap in figure 11, and only the normal component of the field enters the problem. Then a procedure similar to Jaffé's is necessary to generalize the result to arbitrary angles. That is, one can follow the procedure leading to equation (13), except that the integral is evaluated numerically.

The code calculates the positive and negative charge densities from equation (7) for each point in the grid at t = zero. Then it calculates

$$\nabla^2 n_{\pm}(i,j) = \frac{n_{\pm}(i+1,j) + n_{\pm}(i-1,j) + n_{\pm}(i,j+1)}{h^2} + \frac{n_{\pm}(i,j-1) - 4n_{\pm}(i,j)}{h^2} \quad , \tag{24}$$

where i is the x index, j is the y index, and h is the grid spacing. Then the code calculates $\partial n/\partial x$ at each point from the relation

$$\frac{\partial n_{\pm}(i,j)}{\partial x} = \frac{n_{\pm}(i+1,j) - n_{\pm}(i-1,j)}{2h} \quad . \tag{25}$$

The derivatives $\partial n_{\pm}/\partial t$ are calculated at each point by using equation (15). Then the charge densities are updated according to the relation

$$n_{\pm}(i,j,t+\Delta t) = n_{\pm}(i,j,t) + \frac{\partial n_{\pm}(i,j,t)}{\partial t}\,\Delta t \quad , \tag{26}$$

where Δt has to be chosen with some care to keep the problem from becoming unstable. After the new densities have been calculated, an integration routine adds up the surviving charge, and N(t) is printed out. In addition, $\int_0^t N(t')\,dt'$ is calculated after each cycle so that the problem can be generalized to arbitrary angles of incidence. Then the process is repeated by using the new densities and usually a recalculated time step.

This code is extremely simple in that it consists of perhaps 150 FORTRAN statements. However, it requires large amounts of memory and processing time. The grid 200 by 100 means 20,000 grid locations and there are eight variables (n_+, n_-, $\nabla^2 n_+$, $\nabla^2 n_-$, $\partial n_+/\partial x$, $\partial n_-/\partial x$, $\partial n_+/\partial t$, and $\partial n_-/\partial t$) calculated at each point. Thus, there are ~160,000 variables calculated per cycle for several hundred cycles. On an IBM System/370 Model 168 computer, this code requires about 1.4 Mbytes and perhaps 10 to 15 min of run time. (For a complete source listing, see appendix A.)

In the calculations presented here, the following constants were used:

$N_0 = 1.33 \times 10^8$ cm^{-1} for α particles and 2.97×10^7 cm^{-1} for protons,

$\mu_+ = 10^{-5}$ cm^2/V-s,

$\mu_- = 40$ cm^2/V-s,

$\alpha = (\mu_+ + \mu_-)e/\varepsilon\varepsilon_0 = 1.88 \times 10^{-5}$ cm^3/s,

$D_+ = \mu_+ kT/e = 6.5 \times 10^{-8}$ cm^2/s,

$D_- = \mu_- kT/e = 0.261$ cm^2/s,

$b = 3.5$ nm, free parameter chosen to produce agreement with experiment.

The distribution of charges at $t = 0$ is shown in figure 15. In figures 16 to 21, the distributions are shown for $t = 10^{-15}$, 10^{-14}, 3×10^{-14}, 10^{-13}, and 3×10^{-13} s for a perpendicular field of 10^6 V/cm. One can see that the positive charges do not move, and most of the charge recombines before the field separates the negative charges from them. For a much smaller field, $E = 10^4$ V/cm, the distribution at $t = 3 \times 10^{-13}$ s is shown in figure 22. One can see that diffusion of the negative charges is important because the distribution has spread out. The field has moved the negative charges only slightly to the left, but the recombination has eaten away both charge distributions in the region where they still overlap. Figures 23 to 30 show the charge distributions after they have been separated or nearly separated at different fields for incident α particles. One can see from the figures how the yield decreases with decreasing field.

These results are summarized in figure 31, in which the solid line joins the calculated yield values for α particles incident at 45 deg and the experimental points are shown for comparison. One can see that the agreement between theory and experiment is very good if one assumes a column radius of 3.5 nm, especially at high fields. At low fields, the measured yield is slightly higher than calculated, however.

This difference at low fields is probably due to the form of the diffusion coefficient that was used. D was calculated from the relation

$$\frac{D}{\mu} = \frac{kT}{e} \quad , \tag{27}$$

where μ was measured. This relation is valid only for relatively dilute solutions. In this case, the maximum ionization density at t = 0 is extremely high, between 10^{20} and 10^{21} charges/cm^3. Thus, some form of concentration dependent diffusion model[47] or a hot electron model probably is appropriate. Such a model would increase the diffusion term and the yield at low fields where diffusion is already most significant. Crank suggests no less than 10 examples of concentration dependent models that one might choose. There is no physical reason for preferring one of them over another, but they all would produce a correction in the right direction here.

In figure 32, the results of the calculation are compared with the measurements for α particles incident at 6 deg. In the exposures at 6 deg, the normal component of the field is only about 1/10 of the parallel component. For this reason, the cylinders move apart more slowly than they move past each other, and there is a high recombination rate for a relatively long time, at least where the charge distributions still overlap. In this case, the effects at the end of the column of charge have to be specifically accounted for because most of the positive charge that escapes recombination is near the Si-SiO_2 interface.

N(t) for a total field of 0.94 MV/cm is plotted on a log t scale (fig. 33) and on a linear t scale (fig. 34). The time scale can be converted to a position scale if one multiplies by $\mu E_{parallel}$. The charge near the Si-SiO_2 interface contributes more to the observed threshold voltage shift. This effect can easily be accounted for, and the experimental results in figure 32 have been corrected accordingly. Even so, one can see that the measured yield is still higher than the calculated yield. The probable explanation is that some form of concentration dependent diffusion is again appropriate.

The results of the proton calculation are compared with the results of the experiment in figure 35 for an assumed column radius of 3.5 nm. Once again, the agreement is reasonably good. The results of all the calculations are summarized in table 5, in which $T = (L/\cos\theta)/\mu E$ and the yield is $(1/N_0T)\int_0^T N(t)\,dt$.

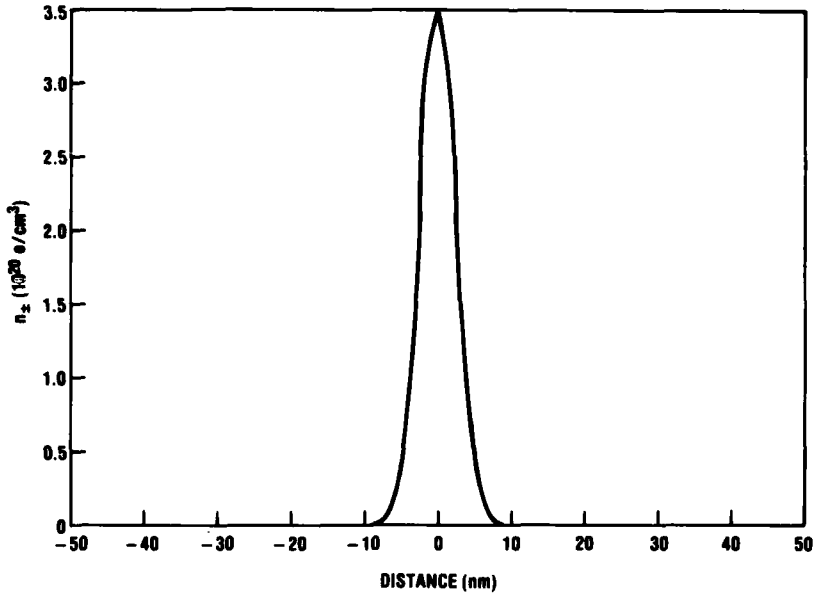

Figure 15. Initial (time = 0) distribution of both positive and negative charges in finite difference solution to "exact" Jaffé equation for perpendicular field = 10^6 V/cm.

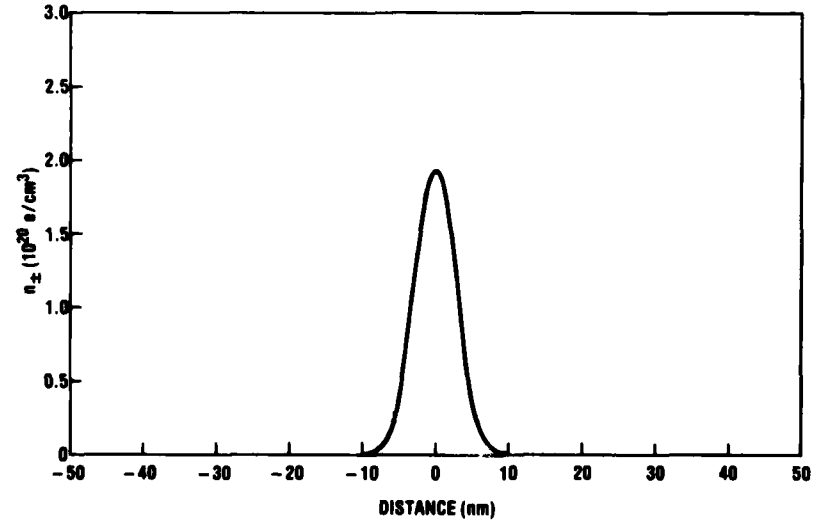

Figure 16. Positive and negative charge densities at time = 10^{-16} s in finite difference calculation for perpendicular field = 10^6 V/cm.

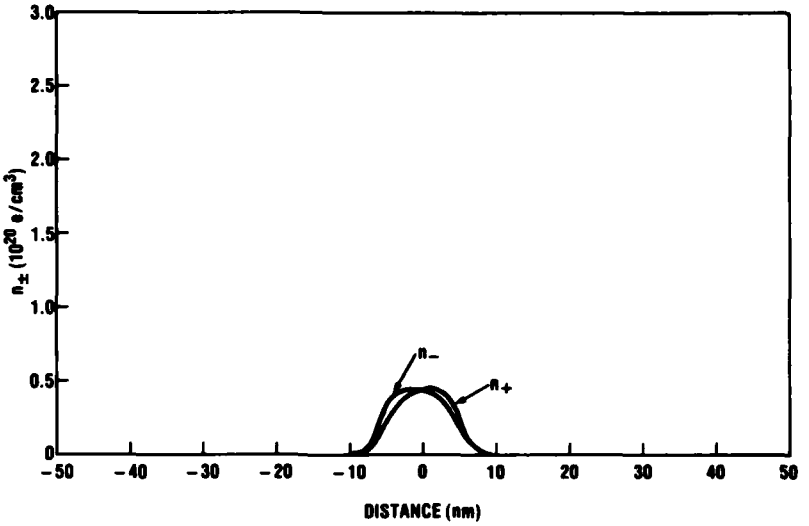

Figure 17. Positive and negative charge densities at time = 10^{-15} s in finite difference calculation for perpendicular field = 10^6 V/cm.

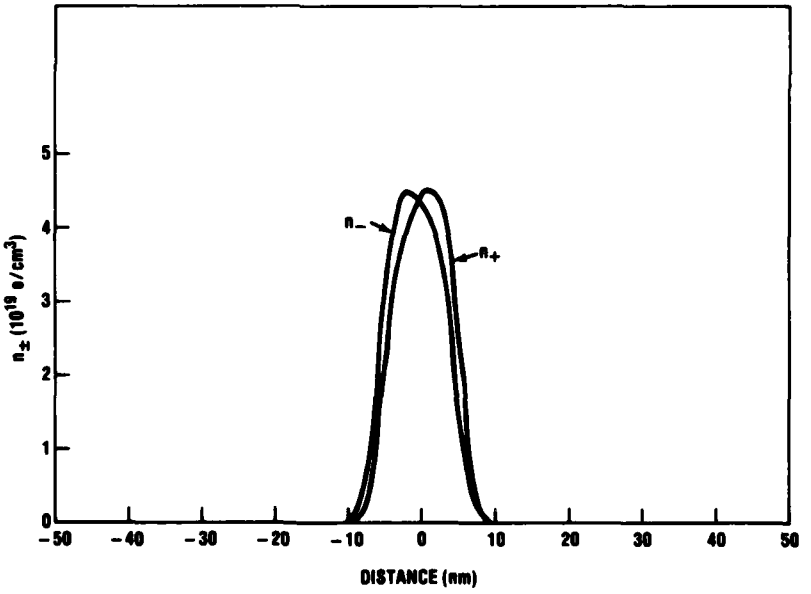

Figure 18. Positive and negative charge densities at time = 10^{-15} s in finite difference calculation for perpendicular field = 10^6 V/cm (fig. 17 replotted on expanded scale).

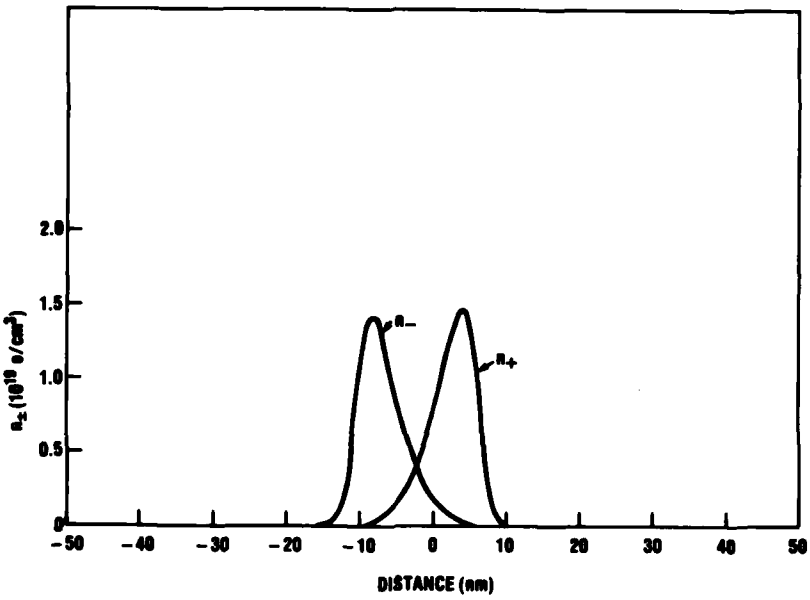

Figure 19. Positive and negative charge densities at time = 10^{-14} s in finite difference calculation for perpendicular field = 10^6 V/cm.

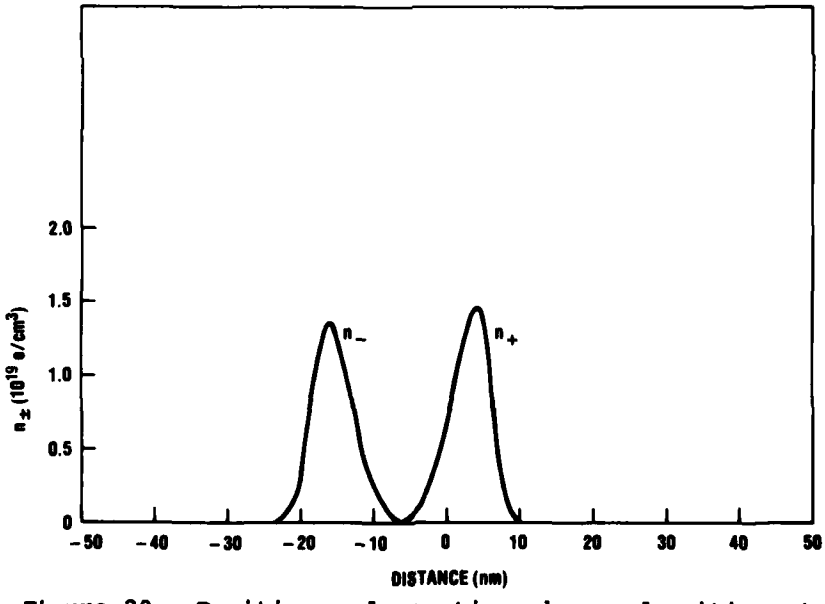

Figure 20. Positive and negative charge densities at time = 3×10^{-14} s for perpendicular field = 10^6 V/cm in finite difference calculation.

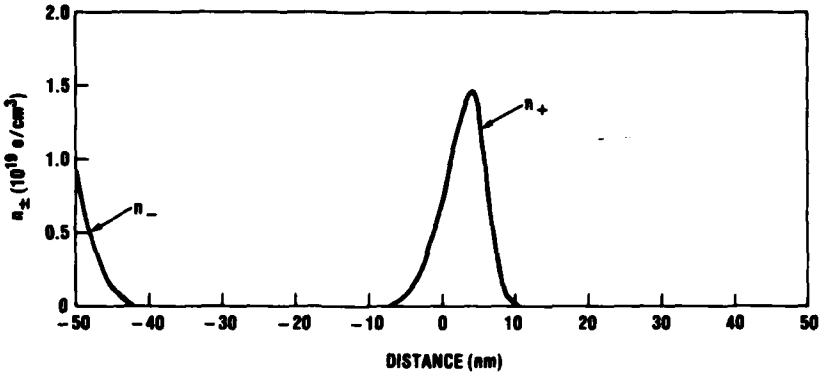

Figure 21. Positive and negative charge densities at time = 10^{-13} s for perpendicular field = 10^6 V/cm in finite difference calculation.

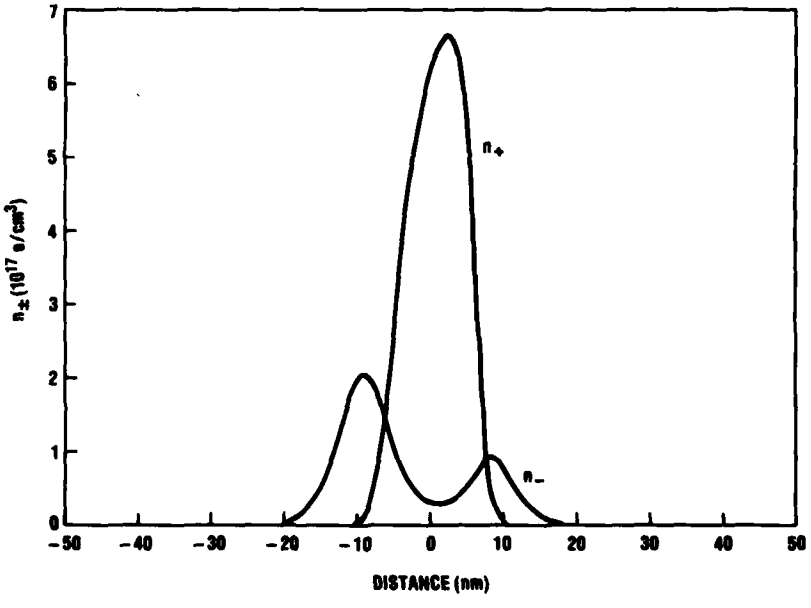

Figure 22. Positive and negative charge densities at time = 3 x 10^{-13} s for perpendicular field = 10^4 V/cm in finite difference calculation (shows importance of diffusion at low fields).

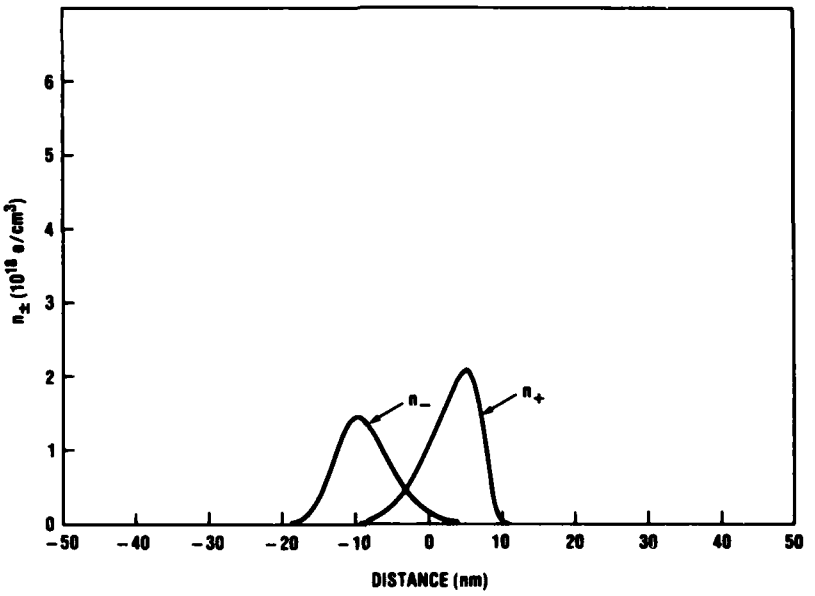

Figure 23. Positive and negative charge densities at time = 10^{-13} s for perpendicular field = 10^5 V/cm.

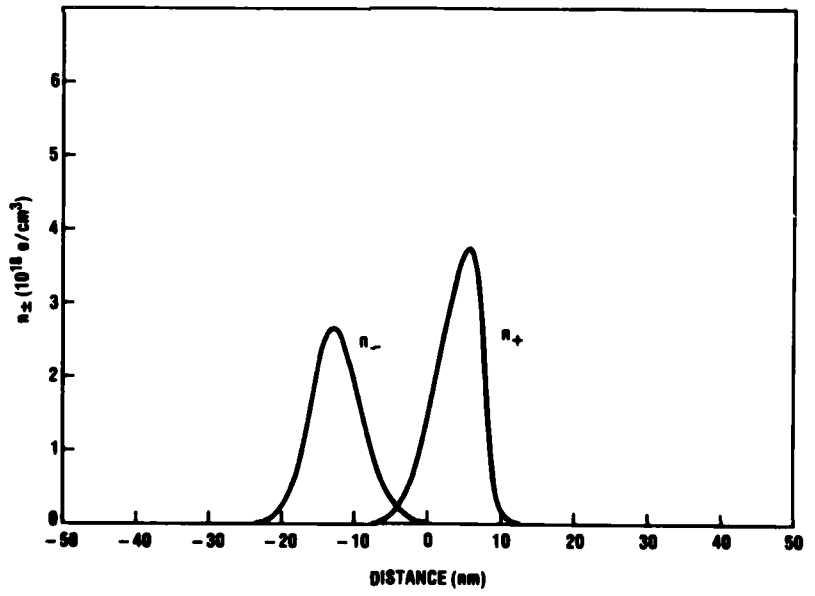

Figure 24. Positive and negative charge distributions at time = 10^{-13} s for perpendicular field = 2×10^5 V/cm.

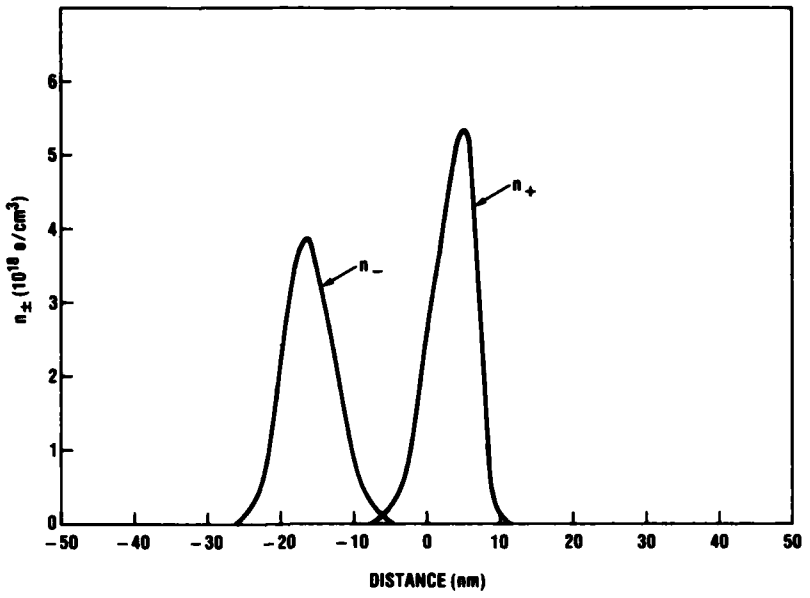

Figure 25. Positive and negative charge densities at time = 10^{-13} s for perpendicular field = 3 × 10^5 V/cm.

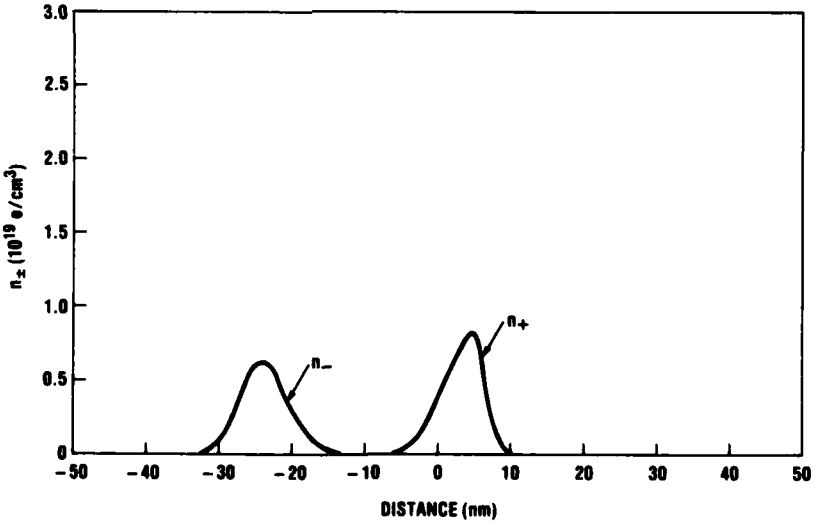

Figure 26. Positive and negative charge distributions at time = 10^{-13} s for perpendicular field = 5 × 10^5 V/cm.

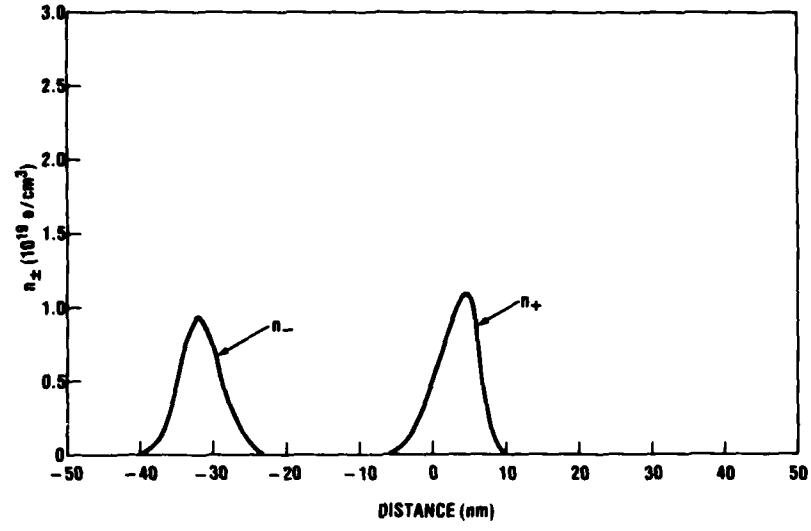

Figure 27. Positive and negative charge distributions at time = 10^{-13} s for perpendicular field = 7×10^5 V/cm.

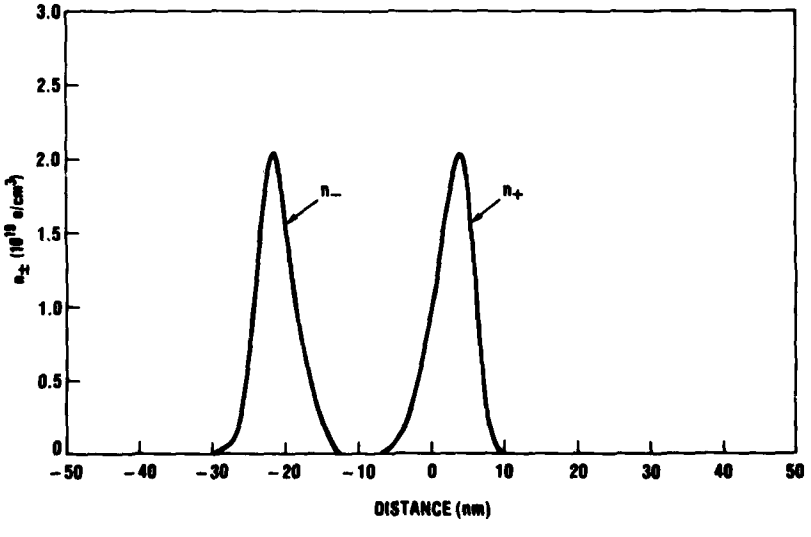

Figure 28. Positive and negative charge distributions at time = 3×10^{-14} s for perpendicular field = 1.5×10^6 V/cm.

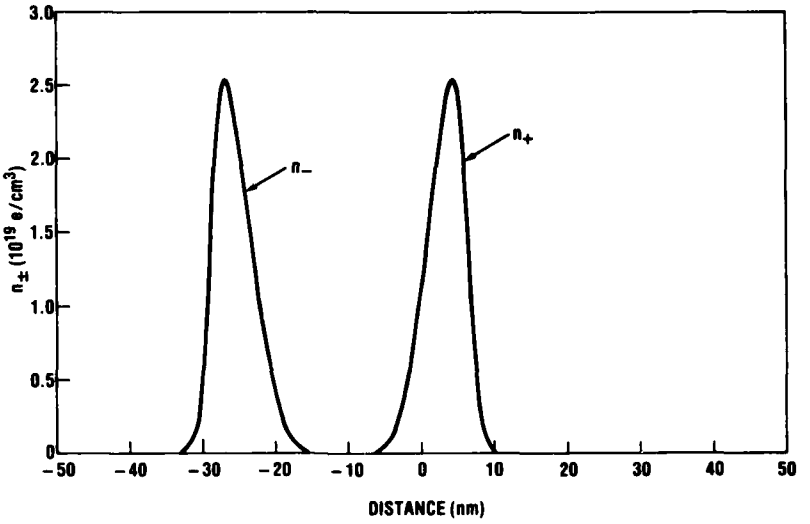

Figure 29. Positive and negative charge distributions at time = 3×10^{-14} s for perpendicular field = 2×10^6 V/cm.

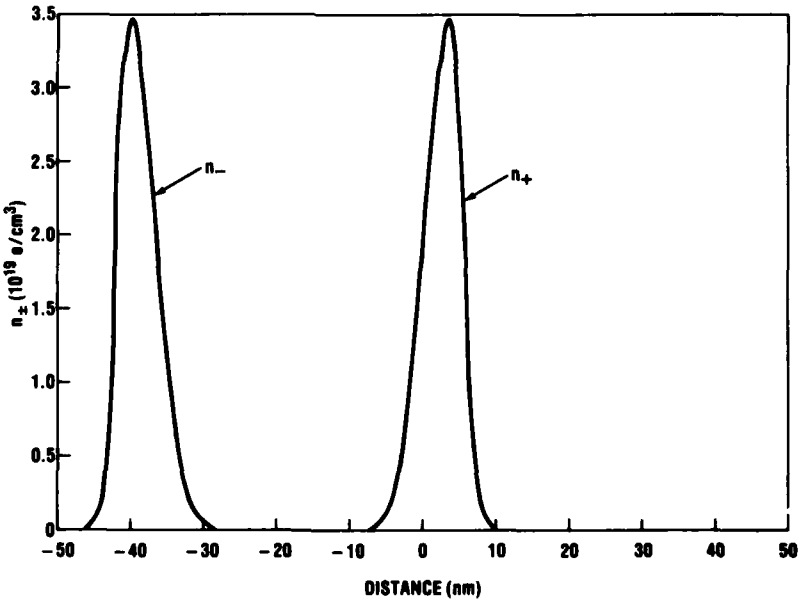

Figure 30. Positive and negative charge distributions at time = 3×10^{-14} s for perpendicular field = 3×10^6 V/cm.

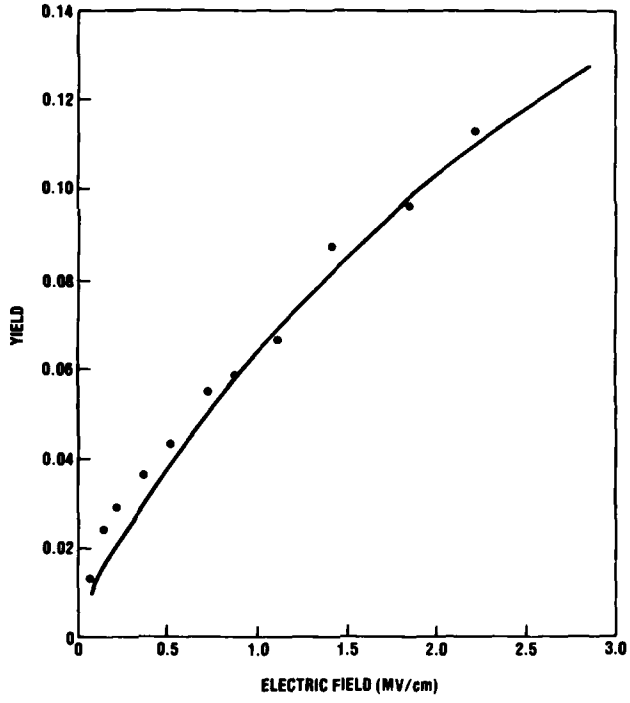

Figure 31. Experimental results for α particles at 45 deg (dots) repeated along with results of finite difference calculation (solid line).

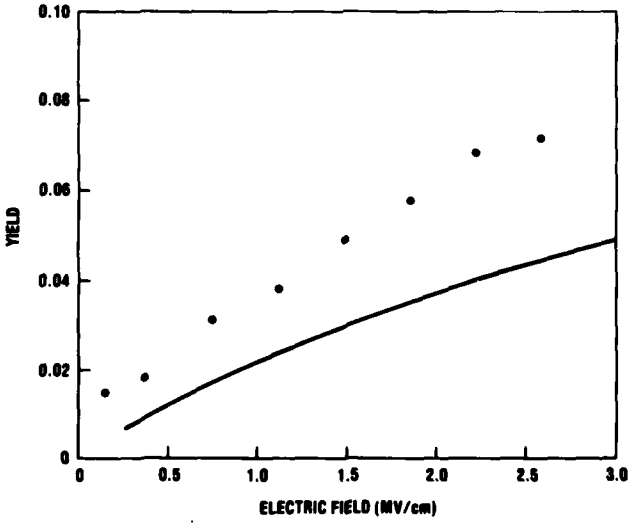

Figure 32. Experimental results for α particles at 6 deg (dots) compared with results of finite difference calculation (solid line).

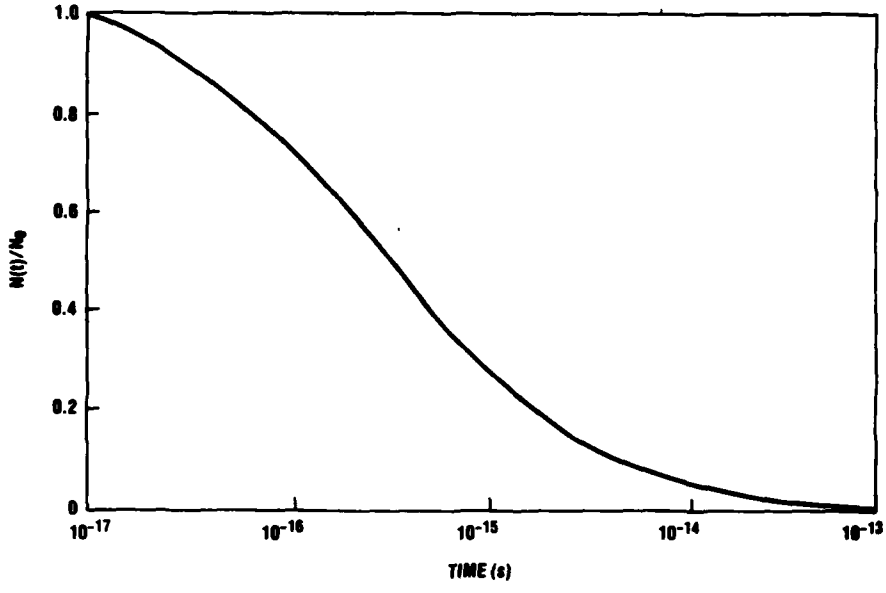

Figure 33. Fraction of charge surviving at time t for perpendicular field = 10^5 V/cm.

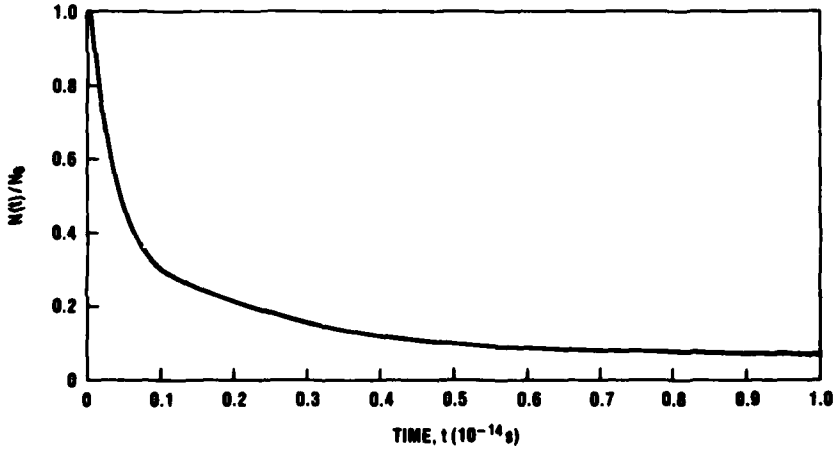

Figure 34. Fraction of charge surviving at time t for perpendicular field = 10^5 V/cm (fig. 33 replotted on linear scale).

Figure 35.

Comparison of proton experimental results with results of finite difference calculation for column radius, b, = 3 and 3.5 nm.

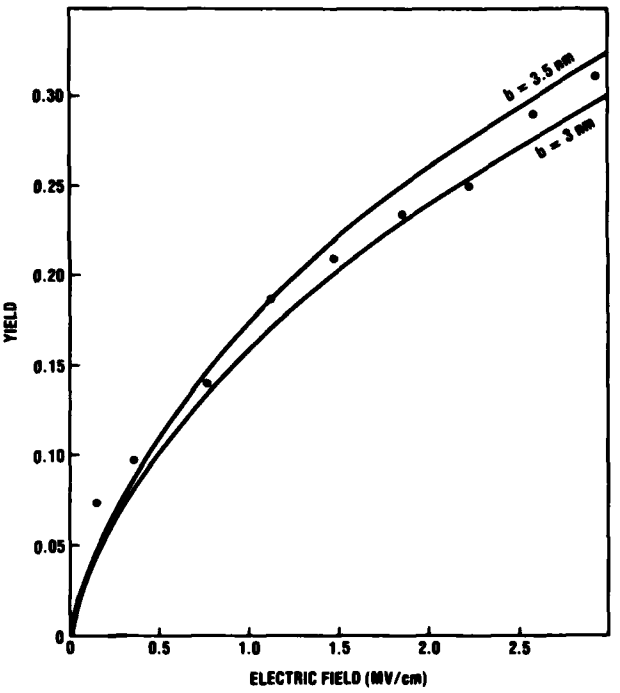

TABLE 5. SUMMARY OF FINITE DIFFERENCE CALCULATION RESULTS

Unit	Normal field (MV/cm)	Total field (MV/cm)	Time (s)	$\int_0^T N(t)\,dt$	Fractional yield
α particle, 45 deg	0.1	0.14	4.73×10^{-12}	9.17×10^{-6}	0.0146
	0.2	0.28	2.36×10^{-12}	7.71×10^{-6}	0.0246
	0.3	0.42	1.58×10^{-12}	7.01×10^{-6}	0.0334
	0.5	0.71	9.45×10^{-13}	6.14×10^{-6}	0.0489
	0.7	0.99	6.75×10^{-13}	5.59×10^{-6}	0.0623
	1.0	1.41	4.73×10^{-13}	5.06×10^{-6}	0.0804
	1.5	2.12	3.15×10^{-13}	4.42×10^{-6}	0.1055
	2.0	2.83	2.36×10^{-13}	4.01×10^{-6}	0.1278
	3.0	4.24	1.58×10^{-13}	3.49×10^{-6}	0.1661
α particle, 6 deg	0.1	0.94	3.59×10^{-13}	0.996×10^{-6}	0.0208
	0.2	1.89	1.79×10^{-13}	0.822×10^{-6}	0.0345
	0.3	2.83	1.19×10^{-13}	0.729×10^{-6}	0.0461
Proton, 45 deg	0.1	0.14	4.73×10^{-12}	6.43×10^{-6}	0.0458
	0.2	0.28	2.36×10^{-12}	5.21×10^{-6}	0.0743
	0.3	0.42	1.58×10^{-12}	4.60×10^{-6}	0.0981
	0.5	0.71	9.45×10^{-13}	3.87×10^{-6}	0.1378
	0.7	0.99	6.75×10^{-13}	3.42×10^{-6}	0.1707
	1.0	1.41	4.73×10^{-13}	2.98×10^{-6}	0.2125
	1.5	2.12	3.15×10^{-13}	2.50×10^{-6}	0.2677
	2.0	2.83	2.36×10^{-13}	2.19×10^{-6}	0.3130
	3.0	4.24	1.58×10^{-13}	1.80×10^{-6}	0.3830

5. DISCUSSION

This work shows that the Jaffé model can be used to calculate the ionization of SiO_2 by heavy charged particles. The Jaffé model has two "free" parameters, N_0 and b, but N_0 can be determined independently. This work, in effect, fixes b for α particles and protons in SiO_2 at ~3.5 nm. In figure 35, the proton experimental data are plotted along with the calculations for b = 3 and 3.5 nm to give an idea of the sensitivity of the calculation to variation in b. Similarly, in figure 36, the 45-deg α particle data are replotted along with calculated yield curves for b = 3 and 4 nm as well as b = 3.5 nm. One can see that the b = 3.5 ± 0.5 nm is a reasonable estimate of the error in the measurement of b.

One reasonably might ask why b should be in the range of 3 to 4 nm; a significant body of literature bears on the question. When a charged particle passes through a medium, the dominant energy loss mechanism is the production of plasmons, which subsequently decay to electron-hole pairs.[48,49] For SiO_2, the plasmon energy is approximately

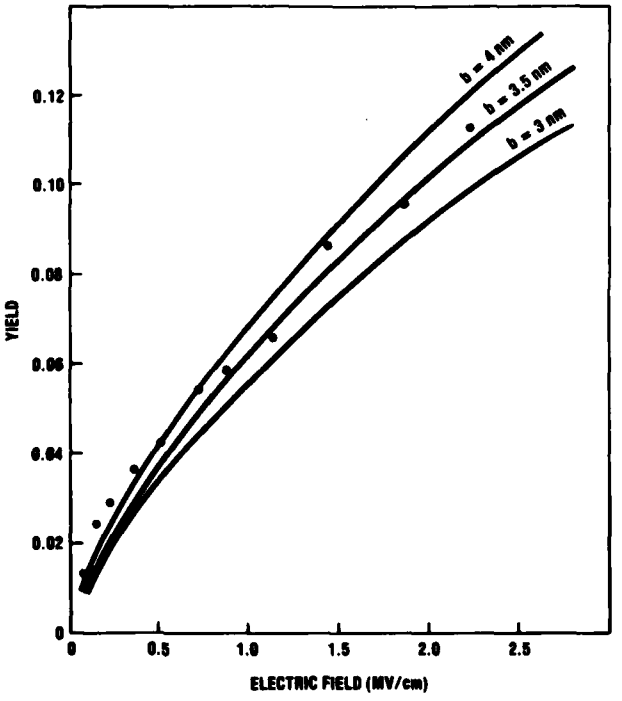

Figure 36. Comparison of α particle experiments with calculations for column radius, b, = 3, 3.5, and 4 nm (indicates how sensitive results are to variation in b).

22 eV ($\omega_p^2 = 4\pi ne^2/m$), and the electron-hole pair energy is approximately 18 eV.[40] This 4 eV, which is lost in thermalization, apparently is lost through the emission of optical phonons having an energy on the order of 0.1 eV.[50-53] The mean free path for phonon emission by hot electrons is on the order of 0.1 nm.[54] In other words, the total path length is on the order of 4 nm (40 events that are 0.1 nm apart). But since the electron-hole pair is on a random walk, the effective thermalization radius is on the order of $\sqrt{40}$ times 0.1 nm or perhaps 0.6 nm, clearly less than 3.5 nm. However, if one takes the uncertainty in the thermal energy of the charges to be on the order of kT, one can calculate $(\Delta p)^2/2m \sim kT$ or $\Delta p \sim 4 \times 10^{-21}$ g-cm/s. Then from the uncertainty principle, $\Delta p \Delta x \gtrsim h$ or $\Delta x \gtrsim 2.4$ nm. Of course, the uncertainty principle gives only an order of magnitude estimate, so one should probably conclude from the argument only that b will fall somewhere about 10^{-6} or 10^{-7} cm. Certainly, the experimentally determined value b = 3.5 nm is within this range.

Similarly, one can estimate the spatial extent of a plasmon. A plasmon is basically a k = 0 excitation, except that the quantum mechanical uncertainty is $k_{min}^2 = 4\pi ne^2 = m_e(22 \text{ eV})$.[55] One can then calculate $\Delta x_{min} \sim 3 \times 10^{-8}$ cm or roughly an order of magnitude less than the extent of the electron wave function. Thus, the extent of the cylinders of charge seems to be determined by the extent of the electron wave functions. In other words, the radius of the cylinders is zero except that, quantum mechanically, nothing is zero to arbitrary accuracy.

Actually, it is somewhat surprising that the analysis based on equation (15) works out as well as it does since the problem should really be treated quantum mechanically. Equation (15) is descended directly from the Boltzmann transport equation, which is usually described as semiclassical and which assumes, for example, that the duration of the collisions is small compared with the mean free time between collisions. If the field is taken to be 10^6 V/cm, then the drift velocity saturates at $\sim 2 \times 10^7$ cm/s. If the mean free path is taken to be 0.1 nm again, then the mean free time is on the order of 10^{-16} s. It is difficult to see how the scattering time could be negligibly small compared with 10^{-16} s.

In addition, thermalization is assumed to be instantaneous, but the actual thermalization time is probably on the order of 10^{-13} s. For times less than the thermalization time (that is, for hot electrons), D is probably larger than the value given below, and μ is somewhat smaller because of carrier-to-carrier collisions.

In addition, plasma effects such as the shielding of external fields are neglected, although at very high densities ($\sim 10^{20}$ cm^{-3}) these effects should be significant.

In spite of these shortcomings, the theory seems to work reasonably well at predicting the yield of charge in the limit as t becomes large. The main reason seems to be that the recombination proceeds very rapidly at early times. Most of the charge has already recombined before the electrons thermalize and before the external field has had much effect. The screening effects become less significant as the density decreases (that is, the assumptions of the theory become better very rapidly as time increases). One should also note that the final yield does not depend on the precise value of μ since both D and α are assumed proportional to μ.

The classical theory used here consistently underestimates the yield when the normal component of the field is small, both in the 45-deg experiments and at 6 deg and for both α particles and protons. A more complete theoretical treatment with a larger effective D to account for hot electron effects would probably improve the agreement with experiment.

A certain amount of work has been done to develop a full quantum mechanical treatment of transport in semiconductors[56-58] and in dielectrics.[51,59,60] However, the semiclassical model that we use here is empirically effective in explaining the experimental results, even though we are straining the assumptions on which the model rests. It is interesting how often a theoretically shaky semiclassical model gives physically reasonable results to quantum mechanical problems--the Rutherford scattering cross section for electrons and the Bohr atomic theory are two other examples.

The experiments and the analysis described above establish that the Jaffé model works reasonably well for α particles and protons. One can easily use the model to calculate the ionization of SiO_2 by other particles or at other energies since these factors enter the calculation only through N_0, the number of electron-hole pairs per unit path length. In table 6, we present calculated results for the cosmic ray nuclei ^{12}C and ^{56}Fe along with our typical α particle and proton results. The energies chosen for ^{12}C and ^{56}Fe correspond to the maximum ionization for those particles, and the α particle and proton energies are chosen to match our experimental conditions. One can see from table 6 that the initial ionization density for ^{56}Fe is roughly 25 times greater than for an α particle. But the amount of charge that escapes recombination is only about twice as great for ^{56}Fe. The reason is that the recombination term, $-\alpha n_+ n_-$, is roughly 600 times greater for ^{56}Fe at first, and the extra free charge is eliminated rapidly.

TABLE 6. CALCULATED RESULTS FOR PROTONS, α PARTICLES, ^{12}C, AND ^{56}Fe

Particle	Particle energy, E (MeV)	Energy loss, dE/dx (MeV/g/cm^2)	Electron hole (pairs/cm)	Fractional yield (field = 1.4 MV/cm)	Yield (holes/cm)
^{1}H	0.7	243	2.97×10^{7}	0.2120	6.30×10^{6}
^{4}He	2.0	1,088	1.33×10^{8}	0.0885	1.18×10^{7}
^{12}C	4.0	5,270	6.44×10^{8}	0.0242	1.56×10^{7}
^{56}Fe	100	30,680	3.75×10^{9}	0.0060	2.25×10^{7}

6. IMPLICATIONS FOR MICROELECTRONIC DEVICES

The possibility of permanent failures of electronic devices from single particles is a timely question in view of the current interest in temporary upsets.[1-5] One might reasonably ask how small the devices would have to be before permanent errors would be observed. Recently, Srour et al[61] considered the possibility that a single neutron might cause enough displacement damage to ruin a submicrometer device. In addition, Oldham and McGarrity[62] have presented a worst case calculation indicating that a single α particle might cause enough ionization to cause a device to fail.

This worst case analysis rests on the assumptions that (1) recombination can be neglected and (2) all the charge reaching the interface is trapped there. The assumption of 100-percent trapping is reasonable in some cases,[63] but the assumption of 100-percent yield is clearly unjustified in view of the experimental results presented above. For 100-percent yield, the device discussed by Dennard et al[64] in their well-known scaling law paper (1 × 1 μm with 35-nm-thick SiO_2) would exhibit a threshold voltage shift (ΔV_T) of about 100 mV after being struck by a 2-MeV α particle. However, if recombination were taken into account, the yield would be only 6 to 10 percent in the field range of 1 to 2 MV/cm, and ΔV_T would be only about 6 to 10 mV. Many present day circuits fail when ΔV_T = 100 mV, but they can withstand ΔV_T = 10 mV.

One can calculate ΔV_T as a function of device dimensions starting from equation (6). If the total charge produced by an ionizing particle is given by equation (6), then the charge escaping recombination is $Q = f(E)Q_0$, as before, and the charge trapped at the interface is $f_T f(E)Q_0$, where f_T is the fraction of holes that reach the Si-SiO_2 interface and are trapped there. Then

$$\Delta V_T = \frac{Q}{C_{ox}} = 3.65 \times 10^{-8} \frac{\ell_{ox}^2}{A} \left|\frac{\partial E}{\partial x}\right| f_T f(E) \frac{\text{volts-cm}}{\text{eV}} , \qquad (28)$$

where A is the active area of the device. If we assume a 2-MeV α particle with f(E) = 10 percent (that is, E ≈ 2 MV/cm) and f_T = 100 percent, we can plot equation (28) for devices of different areas as a function of SiO_2 thickness with the results shown in figure 37. The results in this plot do not include short channel radiation effects,[65] which are poorly understood but which may be important. In considering figure 37, one should remember that voltages are scaled down somewhat as devices are reduced in size. For this reason, tolerable ΔV_T also will tend to shrink in the future. On the other hand, we have assumed f_T = 100 percent, which is realistic only for unhardened commercial SiO_2. For hardened SiO_2, the trapping fraction can be reduced by a factor of 10 or perhaps more, and ΔV_T can be reduced by the same factor.

Actually, the calculation of ΔV_T in figure 37 is misleading because we are dividing total trapped charge by total capacitance. In effect, we are assuming that the charge will be trapped uniformly across the active area of the device, but one would really expect a nonuniform spatial distribution of charge as indicated schematically in figure 38.

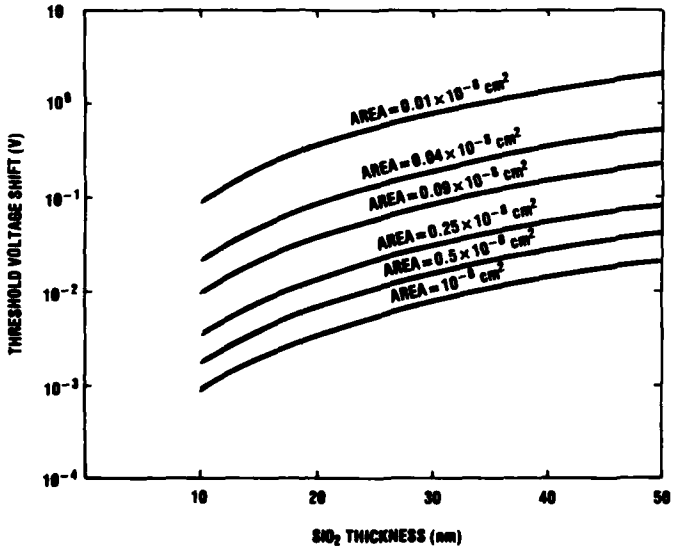

Figure 37. Calculated threshold voltage shift for various small area devices as function of SiO_2 thickness. (This calculation assumes 2-MeV α particle incident at 45 deg and 10-percent yield; that is, applied field ≈ 2 MV/cm. For lower fields or for other particles [protons] or other energies, threshold voltage shift is smaller than shown here.)

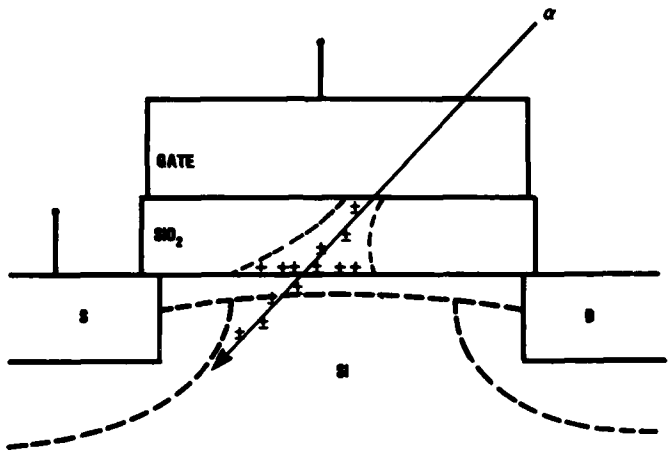

Figure 38. Schematic of MOSFET struck by α particle.

One can do a fairly simple "particle pushing" calculation to estimate the spatial distribution of the charges as they arrive at the interface. We distribute randomly the correct number of positive charges in approximately the correct volume and calculate the coulomb repulsion between each pair of charges. Then following the hole transport model of McLean,[37] we let each hole hop 1 nm parallel to the total field that it sees. Then we stop the particles, recalculate the fields, and let the charges hop again. This process is continued until all the charges are trapped at the interface. The charges generated near the interface reach it first and are trapped near the exit point of the ionizing particle from the SiO_2. As these charges build up, they generate a field that tends to cancel the applied field. Charges arriving later have to spread from the particle track until they are outside the central space charge region, and only then do they move to the interface under the influence of the applied bias.

This process is indicated schematically in figure 39 for an obliquely incident particle. The innermost zone "fills up" first and, as time passes, the remaining zones fill up one at a time in order of increasing distance from where the particle hit, r.

Figure 40 shows the results for an α particle normally incident on SiO_2 100 nm thick, where the applied field is 10^6 V/cm and recombination is neglected. Even though the density at $r < 10$ nm is very high, the total charge in the first zone is only 53 holes in this example. These 53 holes represent a density greater than 10^{13} charges/cm^2, corresponding to an immense field. These holes were created very near the interface, and the field that they generate prevents any more charges from transporting into the $r < 10$ nm zone. Charges arriving later at the interface have to move out to large r before the applied field can drive them to the interface.

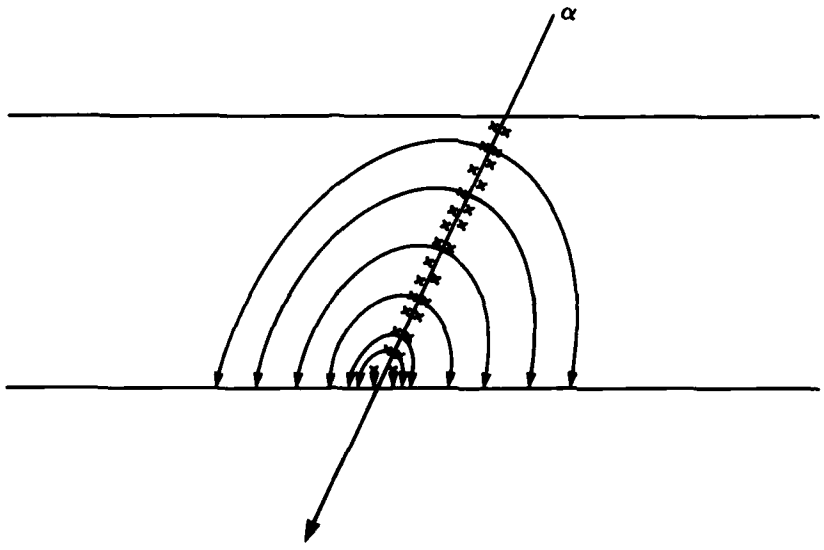

Figure 39. Qualitative illustration of path followed by holes hopping to interface in particle pushing calculation.

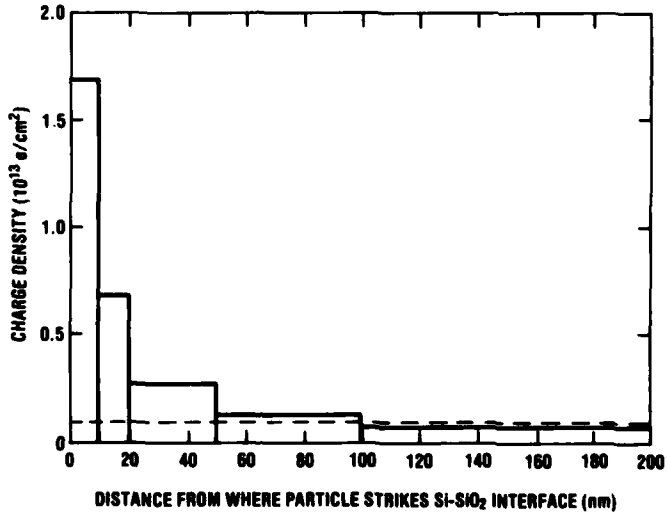

Figure 40. Charge density at interface, assuming normally incident 2-MeV α particle, 100-nm-thick SiO_2, applied field = 10^6 V/cm, and 100-percent yield. (Dashed line shows average [mean] charge density.)

The charge distribution that results from a calculation of this kind depends greatly on the yield. In figures 41 and 42, results are given for ℓ_{ox} = 20 nm, where the field is 10^6 V/cm. The α particle is incident above the origin and exits at x = 20 nm and y = 0. The figures are what one would see looking down from above on the interface, where each dot represents a trapped hole. In figure 41 the yield is 100 percent, but in figure 42 it is only 10 percent. The maximum density is much greater for the higher yield, and the size of the "footprint" also is much greater.

A more realistic case for electronic devices today and in the near future is shown in figure 43. The splatter pattern in figure 43 is for an α particle incident at 45 deg on 50-nm SiO_2, where E = 10^6 V/cm and the yield is assumed to be 10 percent. As before, the particle is incident above the origin, and the exit point is x = 50 nm and y = 0. One can see that the footprint is on the order of 100 nm in diameter, which is much less than the size of a 1-μm device or even a 0.5-μm device. If one imagines this charge distribution placed in a 0.5-μm channel, one can calculate a local flatband voltage shift from the local charge density. There would be a large local shift, but most of the channel would not be affected at all. This result is illustrated in figure 44.

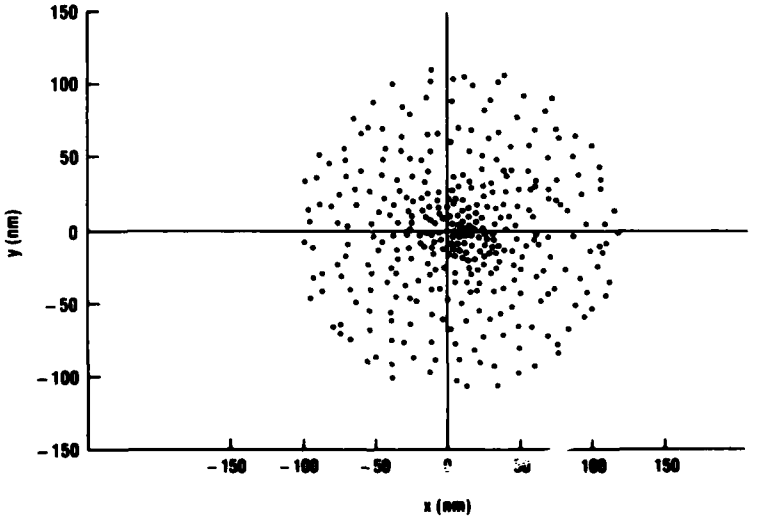

Figure 41. Charge density at interface, assuming that 2-MeV α particle struck 20-nm-thick SiO_2 at 45 deg with applied field = 10^6 V/cm and 100-percent yield. (Each dot represents one trapped hole. Figure shows distribution of holes that one would see looking down from above Si-SiO_2 interface.)

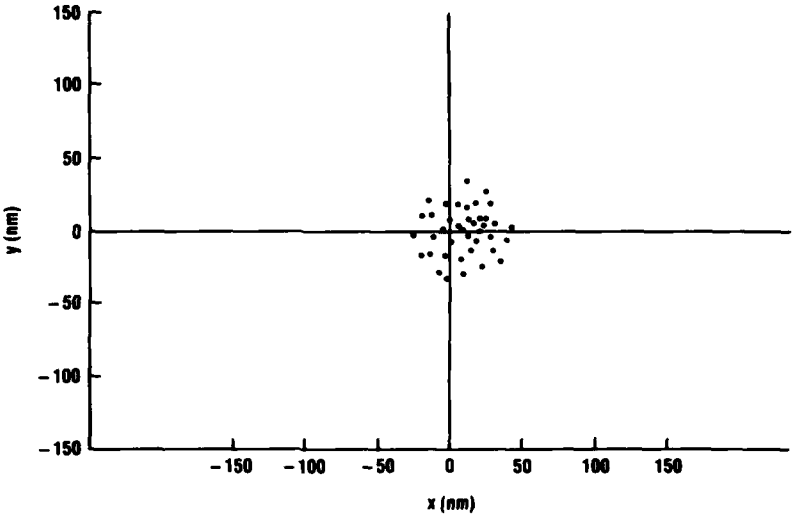

Figure 42. Charge density at interface, assuming that 2-MeV α particle struck 20-nm-thick SiO_2 at 45 deg with applied field = 10^6 V/cm and 10-percent yield. (Each dot represents one trapped hole. Figure shows how spot size depends on yield.)

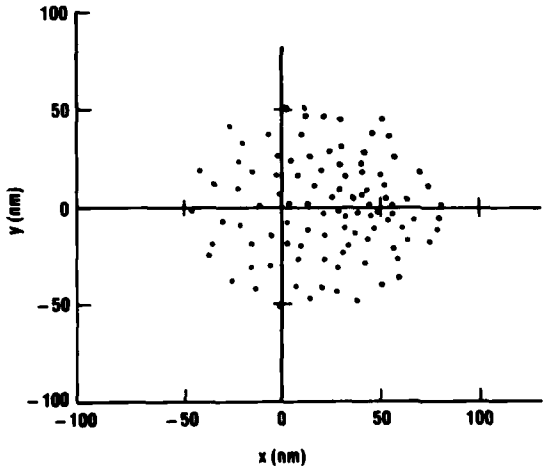

Figure 43.

Charge density at interface, assuming that 2-MeV α particle struck 50-nm-thick SiO_2 at 45 deg with applied field = 10^6 V/cm and 10-percent yield. (Each dot represents one trapped hole. SiO_2 thickness is more nearly typical of present day devices.)

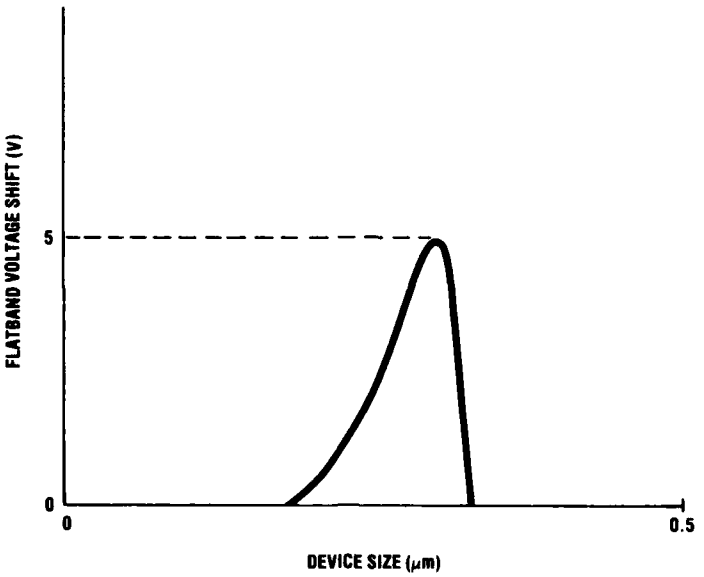

Figure 44. Local flatband voltage shift caused by placing charge distribution in figure 43 in middle of device with 0.5-μm channel length.

Thus, it seems unlikely that a single charged particle will cause a threshold voltage shift large enough to cause a total dose failure in a device, at least until devices are scaled down well below 1 μm. However, the small charge blobs such as in figure 43 could cause unforeseen reliability or stability problems such as punch through or increased hot electron injection. One should remember that highly integrated circuits are increasingly difficult to design and build even in the absence of radiation. Adding a few unexpected blobs of charge to these circuits is a little bit like throwing a handful of sand into a jet engine. The effects are difficult to predict, but they cannot possibly be beneficial.

7. SUMMARY AND CONCLUSIONS

We have measured the recombination of charge produced in SiO_2 by two kinds of heavy charged particles, α particles and protons. The fraction of charge that escapes recombination is relatively small at fields on the order of 1 to 2 MV/cm. The yield for α particles is 10 percent or less, and the yield for protons is 25 percent or less. On the other hand, for relativistic electrons the yield is 90 percent or more at these fields.

The results of these experiments are explained reasonably well by the Jaffé columnar recombination model when a column radius of 3.5 nm is assumed. The Jaffé model is well known, but the column radius for SiO_2 had not previously been determined. Since the column radius is presumably a property of the material, the Jaffé model can now be used to calculate the yield of charge for other particles and other energies.

Finally, the implications of the charge yield measurements for the operation of microelectronic devices are considered. The charge that is produced by an α particle and escapes recombination is unlikely to cause a total dose failure in a device until the devices are much smaller than 1 μm. However, the circuits are complicated enough that the charge from a single α particle could make it more difficult to solve some reliability problems.

ACKNOWLEDGEMENTS

This research was supported jointly by the Defense Nuclear Agency and the Defense Advanced Research Projects Agency. The author thanks Don Simons of the Naval Surface Weapons Center (NSWC), with whose generous cooperation the α particle and proton experiments were able to be performed, and Pat Cady of NSWC for technical assistance with those experiments. The author thanks also Dr. James M. McGarrity of the Harry Diamond Laboratories (HDL), who suggested this work, and Dr. Flynn B. McLean of HDL, for useful technical discussions. The author also especially wishes to thank Dr. James G. Brennan of the Physics Department of the Catholic University of America for useful technical discussions.

LITERATURE CITED

(1) T. C. May and M. H. Woods, Proceedings of 1978 International Reliability Physics Symposium (IRPS), IEEE Catalog No. 78CH12948PA4 (1978), 33-40.

(2) D. J. Redman, R. M. Sega, and R. Joseph, Military Electronics/Countermeasures (March 1980), 42-47; (April 1980), 40-48.

(3) J. F. Ziegler and W. A. Lanford, Science, 206 (1979), 776.

(4) D. H. Phillips, Military Electronics/Countermeasures (August 1979), 88-92; (September 1979), 87-93.

(5) C. S. Guenzer, R. G. Allas, A. B. Campbell, J. M. Kidd, E. L. Peterson, N. Seaman, and E. A. Wolicki, IEEE Trans. Nucl. Sci., NS-27 (1980), 1485-1489.

(6) R. C. Hughes, Solid State Electron., 21 (1978), 251-258.

(7) H. E. Boesch, F. B. McLean, J. M. McGarrity, and P. S. Winokur, IEEE Trans. Nucl. Sci., NS-25 (1978), 1239-1245.

(8) F. B. McLean, G. A. Ausman, H. E. Boesch, and J. M. McGarrity, J. Appl. Phys., 47 (1976), 1259.

(9) J. R. Srour, S. Othmer, O. L. Curtis, and K. Y. Chiu, IEEE Trans. Nucl. Sci., NS-23 (1973), 1513.

(10) R. C. Hughes, Phys. Rev. Lett., 30 (1973), 1333.

(11) C. M. Dozier and D. B. Brown, IEEE Trans. Nucl. Sci., NS-27 (1980), 1694.

(12) W. H. Bragg and R. D. Kleemann, Philos. Mag., 11 (1906), 466.

(13) R. D. Kleemann, Philos. Mag., 12 (1906), 273.

(14) M. von Smoluchowski, Annalen der Physik, 44 (1915), 1103.

(15) L. Onsager, Phys. Rev., 54 (1938), 554.

(16) R. C. Hughes, J. Chem. Phys, 55 (1971), 5442.

(17) K. M. Hong and J. Noolandi, J. Chem. Phys., 68 (1978), 5163.

(18) K. M. Hong and J. Noolandi, J. Chem. Phys., 68 (1978), 5026.

(19) K. M. Hong and J. Noolandi, J. Chem. Phys., 68 (1978), 5172.

(20) G. A. Ausman, Jr., Charge Neutralization and Electron Scavenging in Irradiated Dielectric Liquids, U.S. Army Harry Diamond Laboratories HDL-TR-1662 (April 1974).

(21) R. C. Hughes, J. Chem. Phys., 58 (1973), 2212.

(22) A. Mozumder and J. L. Magee, Radiat. Res., 28 (1966), 203.

(23) A. Mozumder and J. L. Magee, Radiat. Res., 28 (1966), 215.

(24) M. M. Moulin, Ann. Chim. Phys. VIII, 21 (1910), 550.

(25) M. M. Moulin, Ann. Chim. Phys. VIII, 21 (1911), 26.

(26) M. P. Langevin, Ann. Chim. Phys. VII, 28 (1903), 433.

(27) M. P. Langevin, Ann. Chim. Phys. VII, 28 (1903), 289.

(28) G. Jaffé, Annalen der Physik, 42 (1913), 303.

(29) G. Jaffé, Phys. Z., 15 (1914), 353.

(30) G. Jaffé, Phys. Z., 23 (1929), 849.

(31) A. N. Gerritsen, Physica, 14 (1948), 381.

(32) A. N. Gerritsen, Physica, 14 (1948), 407.

(33) H. A. Kramers, Physica, 18 (1952), 665.

(34) H. E. Boesch, F. B. McLean, J. M. McGarrity, and G. A. Ausman, IEEE Trans. Nucl. Sci., NS-22 (1975), 2163.

(35) R. C. Hughes, Phys. Rev. B, 15 (1977), 2012.

(36) R. C. Hughes, IEEE Trans. Nucl. Sci., NS-22 (1975), 2227.

(37) F. B. McLean, H. E. Boesch, and J. M. McGarrity, in The Physics of SiO_2 and Its Interfaces, ed. by S. T. Pantelides, Pergamon Press, Inc., New York (1978), 19.

(38) J. F. Ziegler, The Stopping Power and Ranges of Ions in Matter, 3, 4, 5, Pergamon Press, Inc., New York (1977).

(39) K. H. Zaininger and F. P. Heiman, Solid State Technol., 13 (1970).

(40) G. A. Ausman and F. B. McLean, Appl. Phys. Lett., 26 (1975), 173.

(41) H. H. Sander and B. L. Gregory, IEEE Trans. Nucl. Sci., NS-22 (1975), 2157.

(42) H. E. Boesch and J. M. McGarrity, IEEE Trans. Nucl. Sci., NS-23 (1976), 1520.

(43) O. L. Curtis, J. R. Srour, and K. Y. Chiu, J. Appl. Phys., 45 (1974), 406.

(44) E. Jahnke and F. Emde, Tables of Functions, Dover Publications, Inc., New York (1945).

(45) R. D. Evans, The Atomic Nucleus, McGraw-Hill Book Co., New York (1955).

(46) H. Enge, Introduction to Nuclear Physics, Addison-Wesley Publishing Co., Reading, MA (1966).

(47) J. Crank, The Mathematics of Diffusion, Clarendon Press, Oxford (1975).

(48) D. Pines, Rev. Mod. Phys., 28 (1956), 184.

(49) A. Rothwarf, J. Appl. Phys., 44 (1973), 752.

(50) R. C. Hughes, Phys. Rev. Lett., 35 (1975), 449.

(51) K. K. Thornber and R. P. Feynmann, Phys. Rev. B, 1 (1970), 4099.

(52) D. K. Ferry, Appl. Phys. Lett., 27 (1975), 689.

(53) W. T. Lynch, J. Appl. Phys., 43 (1972), 3274.

(54) R. C. Hughes, Solid State Electron., 21 (1978), 251.

(55) J. M. Ziman, Electrons and Phonons, Clarendon Press, Oxford (1960).

(56) J. R. Barker and D. K. Ferry, Solid State Electron., 23 (1978), 519.

(57) J. R. Barker and D. K. Ferry, Solid State Electron., 23 (1978), 531.

(58) D. K. Ferry and J. R. Barker, Solid State Electron., 23 (1978), 545.

(59) D. K. Ferry, J. Appl. Phys., 50 (1979), 1422.

(60) K. K. Thornber, Solid State Electron., 21 (1978), 259.

(61) J. R. Srour, S. Othmer, A. Bahraman, and M. A. Hopkins, IEEE Trans. Nucl. Sci., NS-28 (December 1981), 3968.

(62) T. R. Oldham and J. M. McGarrity, Prediction of Single-Particle-Induced Permanent Failures in Microelectronics, U.S. Army Harry Diamond Laboratories HDL-TR-1966 (July 1981).

(63) R. Freeman and A. Holmes-Siedle, IEEE Trans. Nucl. Sci., NS-25 (1978), 1216.

(64) R. H. Dennard, F. H. Gaensslen, Hwa-Nien Yu, V. L. Rideout, E. Bassous, and A. R. LeBlanc, IEEE J. Solid State Circuits, SC-9 (1974), 256.

(65) S. Share and R. A. Martin, IEEE Trans. Electron Devices, ED-22 (1975), 619.

APPENDIX A.--FORTRAN LISTING OF THE FINITE DIFFERENCE CODE

APPENDIX A

The FORTRAN listing of the finite difference code is given below. Subroutine INIT initializes certain variables, subroutine INT integrates the total charge and updates the yield integral, subroutine LAPLAC calculates the Laplacian operator, subroutine DNDX calculates the derivatives $\partial n/\partial x$, subroutine DNDT calculates the derivatives $\partial n/\partial t$, subroutine NTKP1 calculates the new charge densities for the next cycle, and subroutine OUTPUT writes the results. The main program supervises the subroutines.

```
      IMPLICIT REAL*8 (A-H,O-Z)
      COMMON X(201), Y(101) , RHON(201,101), RHOP(201,101)
      COMMON D2RHON(201,101), D2RHOP(201,101), DDXRHN(201,101)
      COMMON DDXRHP(201,101), DNNDT(201,101), DNPDT(201,101),TPRINT(10)
      COMMON E,B,DN,DP,ALPHA,RHOL,UN,UP,TOTN,TOTP,DELTO,DELT, TRATIO
      COMMON T,DELX,DELY,YIELD,NPRINT,IPRINT,K
      COMMON NXMAX,NYMAX,NTMAX,NMAX,NXMXM1,NYMXM1,JMIN,JMAX,IFLAG
      CALL INIT
      CALL INT
      CALL OUTPUT
      DO 200 K=1,NTMAX
      CALL LAPLAC
      CALL DNDX
      CALL DNDT
      CALL NTKP1
      CALL INT
      CALL OUTPUT
      T=T+DELT
      DELT=TRATIO*DELT
      IF (IFLAG.GT.NPRINT) GO TO 201
  200 CONTINUE
  201 STOP
      END
```

APPENDIX A

```
      SUBROUTINE INIT
      IMPLICIT REAL*8 (A-H,O-Z)
      COMMON X(201), Y(101) , RHON(201,101), RHOP(201,101)
      COMMON D2RHON(201,101), D2RHOP(201,101), DDXRHN(201,101)
      COMMON DDXRHP(201,101), DNNDT(201,101), DNPDT(201,101),TPRINT(10)
      COMMON E,B,DN,DP,ALPHA,RHOL,UN,UP,TOTN,TOTP,DELTO,DELT, TRATIO
      COMMON T,DELX,DELY,YIELD,NPRINT,IPRINT,K
      COMMON NXMAX,NYMAX,NTMAX,NMAX,NXMXM1,NYMXM1,JMIN,JMAX,IFLAG
      READ (5,100) E,B,DN,DP,ALPHA,RHOL,UN,UP
      READ (5,100) DELX,DELY,DELTO,TRATIO
      READ (5,101) NXMAX,NYMAX,NTMAX,NPRINT,JMIN,JMAX
      READ (5,100) (TPRINT(I),I=1,NPRINT)
  100 FORMAT (9D10.3)
  101 FORMAT (6I10)
      WRITE (6,102)
  102 FORMAT (1H1)
      WRITE (6,103) E,B,DN,DP,UN,UP,ALPHA,RHOL
  103 FORMAT (' E=',D10.3,5X,' B= ',D10.3,5X,' DN= ',D10.3,5X,' DP= ',
     X  D10.3,5X,' UN= ',D10.3,5X,' UP= ',D10.3,5X,//,' ALPHA= ',D10.3,
     X  5X,' RHOL= ',D10.3)
      WRITE (6,104) DELX,DELY,DELTO,TRATIO
  104 FORMAT ('  DELX=',D10.3,5X,' DELY= ',D10.3,5X,' DELTO= ',D10.3,5X,
     X    ' TRATIO=',D10.3)
      WRITE (6,105) NXMAX,NYMAX,NTMAX,NPRINT,JMIN,JMAX
  105 FORMAT (' NXMAX= ',I6,6X,' NYMAX= ',I6,6X,' NTMAX=', I6,6X,
     X  ' NPRINT= ',I6,6X,' JMIN= ',I6,6X, 'JMAX= ',I6)
      WRITE (6,106) (TPRINT(I),I=1,NPRINT)
  106 FORMAT (' TPRINT= ',10(D10.3,2X))
      NMAX=2*NXMAX-1
      DO 200 I=1,NMAX
      X(I)=(I-NXMAX)*DELX
  200 CONTINUE
      Y(1)= 0.D0
      DO 203 J=2,NYMAX
      Y(J)= (J-1)*DELY
  203 CONTINUE
      DO 201 J=1,NYMAX
      DO 201 I=1,NMAX
      RSQ=-(X(I)**2+Y(J)**2)/B**2
      IF (RSQ.LT.-100.D0) GO TO 204
      RHON(I,J)= (RHOL/(3.14159*B*B))*DEXP(-(X(I)**2+Y(J)**2)/B**2)
      RHOP(I,J)=RHON(I,J)
      GO TO 205
  204 RHON(I,J)=0.D0
      RHOP(I,J)=0.D0
  205 D2RHON(I,J)=0.D0
      D2RHOP(I,J)=0.D0
      DDXRHN(I,J)=0.D0
      DDXRHP(I,J)=0.D0
  201 CONTINUE
      IFLAG=0
      IPRINT=0
      T=0.D0
      DELT=DELTO
      YIELD =0.D0
      RETURN
      END
```

```
      SUBROUTINE LAPLAC
      IMPLICIT REAL*8 (A-H,O-Z)
      COMMON X(201), Y(101) , RHON(201,101), RHOP(201,101)
      COMMON D2RHON(201,101), D2RHOP(201,101), DDXRHN(201,101)
      COMMON DDXRHP(201,101), DNNDT(201,101), DNPDT(201,101),TPRINT(10)
      COMMON E,B,DN,DP,ALPHA,RHOL,UN,UP,TOTN,TOTP,DELTO,DELT, TRATIO
      COMMON T,DELX,DELY,YIELD,NPRINT,IPRINT,K
      COMMON NXMAX,NYMAX,NTMAX,NMAX,NXMXM1,NYMXM1,JMIN,JMAX,IFLAG
      NXMXM1=NMAX-1
      NYMXM1=NYMAX-1
      D2RHON(1,1)= (RHON(2,1)+RHON(1 ,2)-2*RHON(1,1))/DELX**2
      D2RHOP(1,1)= (RHOP(2,1)+RHOP(1 ,2)-2*RHOP(1,1))/DELX**2
      DO 200 J=2,NYMXM1
      D2RHON(1,J)=(RHON(2,J)+RHON(1 ,J-1)+RHON(1,J+1)-3*RHON(1,J))/
     X  DELX**2
      D2RHOP(1,J)=(RHOP(2,J)+RHOP(1 ,J-1)+RHOP(1,J+1)-3*RHOP(1,J))/
     X  DELX**2
  200 CONTINUE
      D2RHON(1,NYMAX)=(RHON(2,NYMAX)+RHON(1,NYMXM1)-2*RHON(1,NYMAX))/
     X  DELX**2
      D2RHOP(1,NYMAX)=(RHOP(2,NYMAX)+RHOP(1,NYMXM1)-2*RHOP(1,NYMAX))/
     X  DELX**2
      DO 201 I=2 ,NXMXM1
      D2RHON(I,1)=(RHON(I+1,1)+RHON(I-1 ,1)+2*RHON(I,2)-4*RHON(I,1))/
     X  DELX**2
      D2RHOP(I,1)=(RHOP(I+1,1)+RHOP(I-1 ,1)+2*RHOP(I,2)-4*RHOP(I,1))/
     X  DELX**2
      D2RHON(I,NYMAX)=(RHON(I+1,NYMAX)+RHON(I-1,NYMAX)+RHON(I,NYMXM1)-
     X  3*RHOP(I,NYMAX))/DELX**2
      D2RHOP(I,NYMAX)=(RHOP(I+1,NYMAX)+RHOP(I-1,NYMAX)+RHOP(I,NYMXM1)-
     X  3*RHON(I,NYMAX))/DELX**2
  201 CONTINUE
      DO 202 J=2,NYMXM1
      DO 202 I=2,NXMXM1
      D2RHON(I,J)=(RHON(I-1,J)+RHON(I+1,J)+RHON(I,J+1)+RHON(I,J-1)-
     X  4*RHON(I,J))/DELX**2
      D2RHOP(I,J)=(RHOP(I-1,J)+RHOP(I+1,J)+RHOP(I,J+1)+RHOP(I,J-1)-
     X  4*RHOP(I,J))/DELX**2
  202 CONTINUE
      D2RHON( NMAX,1)=(RHON(NXMXM1,1)+RHON( NMAX,2)-2*RHON( NMAX,1))/
     X  DELX**2
      D2RHOP( NMAX,1)=(RHOP(NXMXM1,1)+RHOP( NMAX,2)-2*RHOP(NMAX, 1))/
     X  DELX**2
      D2RHON( NMAX,NYMAX)=(RHON(NXMXM1,NYMAX)+RHON( NMAX,NYMXM1)-2*RHON
     X  ( NMAX,NYMAX))/DELX**2
      D2RHOP( NMAX,NYMAX)=(RHOP(NXMXM1,NYMAX)+RHOP( NMAX,NYMXM1)-2*RHOP
     X  ( NMAX,NYMAX))/DELX**2
      DO 203 J=2,NYMXM1
      D2RHON( NMAX,J)= (RHON(NXMXM1,J)+RHON( NMAX,J-1)+RHON( NMAX,J+1)-
     X  3*RHON( NMAX,J))/DELX**2
      D2RHOP( NMAX,J)= (RHOP(NXMXM1,J)+RHOP( NMAX,J-1)+RHOP( NMAX,J+1)-
     X  3*RHOP(NMAX, J))/DELX**2
  203 CONTINUE
      RETURN
      END
```

APPENDIX A

```
      SUBROUTINE DNDX
      IMPLICIT REAL*8 (A-H,O-Z)
      COMMON X(201), Y(101) , RHON(201,101), RHOP(201,101)
      COMMON D2RHON(201,101), D2RHOP(201,101), DDXRHN(201,101)
      COMMON DDXRHP(201,101), DNNDT(201,101), DNPDT(201,101),TPRINT(10)
      COMMON E,B,DN,DP,ALPHA,RHOL,UN,UP,TOTN,TOTP,DELTO,DELT, TRATIO
      COMMON T,DELX,DELY,YIELD,NPRINT,IPRINT,K
      COMMON NXMAX,NYMAX,NTMAX,NMAX,NXMXM1,NYMXM1,JMIN,JMAX,IFLAG
      DO 200 J=1,NYMAX
      DDXRHN(1 ,J)=(RHON(2,J)-RHON(1,J))/DELX
      DDXRHP(1 ,J)=(RHOP(2,J)-RHOP(1,J))/DELX
      DDXRHN( NMAX,J)=(RHON( NMAX,J)-RHON(NXMXM1,J))/DELX
      DDXRHP( NMAX,J)=(RHOP( NMAX,J)-RHOP(NXMXM1,J))/DELX
  200 CONTINUE
      DO 202 J=1,NYMAX
      DO 201 I=2,NXMXM1
      DDXRHN(I,J)=(RHON(I+1,J)-RHON(I-1,J))/(2*DELX)
      DDXRHP(I,J)=(RHOP(I+1,J)-RHOP(I-1,J))/(2*DELX)
  201 CONTINUE
  202 CONTINUE
      RETURN
      END
```

```
      SUBROUTINE DNDT
      IMPLICIT REAL*8 (A-H,O-Z)
      COMMON X(201), Y(101) , RHON(201,101), RHOP(201,101)
      COMMON D2RHON(201,101), D2RHOP(201,101), DDXRHN(201,101)
      COMMON DDXRHP(201,101), DNNDT(201,101), DNPDT(201,101),TPRINT(10)
      COMMON E,B,DN,DP,ALPHA,RHOL,UN,UP,TOTN,TOTP,DELTO,DELT, TRATIO
      COMMON T,DELX,DELY,YIELD,NPRINT,IPRINT,K
      COMMON NXMAX,NYMAX,NTMAX,NMAX,NXMXM1,NYMXM1,JMIN,JMAX,IFLAG
      DO 201 J=1,NYMAX
      DO 200 I=1,NMAX
      DNNDT(I,J)=DN*D2RHON(I,J)+UN*E*DDXRHN(I,J)-ALPHA*RHON(I,J)*
     X  RHOP(I,J)
      DNPDT(I,J)=DP*D2RHOP(I,J)-UP*E*DDXRHP(I,J)-ALPHA*RHON(I,J)*
     X  RHOP(I,J)
  200 CONTINUE
  201 CONTINUE
      RETURN
      END
```

```
      SUBROUTINE NTKP1
      IMPLICIT REAL*8 (A-H,O-Z)
      COMMON X(201), Y(101) , RHON(201,101), RHOP(201,101)
      COMMON D2RHON(201,101), D2RHOP(201,101), DDXRHN(201,101)
      COMMON DDXRHP(201,101), DNNDT(201,101), DNPDT(201,101),TPRINT(10)
      COMMON E,B,DN,DP,ALPHA,RHOL,UN,UP,TOTN,TOTP,DELTO,DELT, TRATIO
      COMMON T,DELX,DELY,YIELD,NPRINT,IPRINT,K
      COMMON NXMAX,NYMAX,NTMAX,NMAX,NXMXM1,NYMXM1,JMIN,JMAX,IFLAG
      DO 201 J=1,NYMAX
      DO 200 I=1, NMAX
      RHON(I,J)=RHON(I,J)+DNNDT(I,J)*DELT
      RHOP(I,J)=RHOP(I,J)+DNPDT(I,J)*DELT
  200 CONTINUE
  201 CONTINUE
      RETURN
      END
```

```
      SUBROUTINE INT
      IMPLICIT REAL*8 (A-H,O-Z)
      COMMON X(201), Y(101) , RHON(201,101), RHOP(201,101)
      COMMON D2RHON(201,101), D2RHOP(201,101), DDXRHN(201,101)
      COMMON DDXRHP(201,101), DNNDT(201,101), DNPDT(201,101),TPRINT(10)
      COMMON E,B,DN,DP,ALPHA,RHOL,UN,UP,TOTN,TOTP,DELTO,DELT, TRATIO
      COMMON T,DELX,DELY,YIELD,NPRINT,IPRINT,K
      COMMON NXMAX,NYMAX,NTMAX,NMAX,NXMXM1,NYMXM1,JMIN,JMAX,IFLAG
      TOTN=0.DO
      TOTP=0.DO
      DO 200 I=1,NMAX
      TOTN= RHON(I,1)*DELX*DELY+TOTN
      TOTP= RHOP(I,1)*DELX*DELY+TOTP
  200 CONTINUE
      DO 201 J=2,NYMAX
      DO 201 I=1,NMAX
      TOTN=2*RHON(I,J)*DELX*DELY+TOTN
      TOTP=2*RHOP(I,J)*DELX*DELY+TOTP
  201 CONTINUE
      YIELD=YIELD+TOTP*DELT
      RETURN
      END
```

APPENDIX A

```
      SUBROUTINE OUTPUT
      IMPLICIT REAL*8 (A-H,O-Z)
      COMMON X(201), Y(101) , RHON(201,101), RHOP(201,101)
      COMMON D2RHON(201,101), D2RHOP(201,101), DDXRHN(201,101)
      COMMON DDXRHP(201,101), DNNDT(201,101), DNPDT(201,101),TPRINT(10)
      COMMON E,B,DN,DP,ALPHA,RHOL,UN,UP,TOTN,TOTP,DELTO,DELT, TRATIO
      COMMON T,DELX,DELY,YIELD,NPRINT,IPRINT,K
      COMMON NXMAX,NYMAX,NTMAX,NMAX,NXMXM1,NYMXM1,JMIN,JMAX,IFLAG
      WRITE (6,101)     K,T,TOTN,TOTP,YIELD
  101 FORMAT (' CYCLE NO= 'I5,5X,' T= ',D10.3,5X,' TOTN= ',D10.3,
     X  5X,' TOTP= ',D10.3,5X,' YIELD= ',D10.3)
      IF (T.GE.TPRINT(IFLAG)) IPRINT=1
      IF (IPRINT.EQ.1) GO TO 201
      GO TO 202
  201 WRITE (6,102)
  102 FORMAT (1H1)
      DO 203 I=1,NMAX
      WRITE (6,103)  ((X(I),Y(J),RHON(I,J),RHOP(I,J)),J=JMIN,JMAX)
  103 FORMAT (' X=',D10.3,5X,' Y=',D10.3,5X,' N= ',D10.3,5X,
     X    ' P= ',D10.3)
  203 CONTINUE
      IPRINT=0
      IFLAG=IFLAG+1
  202 RETURN
      END
```

DISTRIBUTION

ADMINISTRATOR
DEFENSE TECHNICAL INFORMATION CENTER
ATTN DTIC-DDA (12 COPIES)
CAMERON STATION, BUILDING 5
ALEXANDRIA, VA 22314

COMMANDER
US ARMY RSCH & STD GP (EUR)
ATTN CHIEF, PHYSICS & MATH BRANCH
FPO NEW YORK 09510

COMMANDER
US ARMY MISSILE & MUNITIONS
CENTER & SCHOOL
ATTN ATSK-CTD-F
REDSTONE ARSENAL, AL 35809

DIRECTOR
US ARMY MATERIEL SYSTEMS ANALYSIS
ACTIVITY
ATTN DRXSY-MP
ABERDEEN PROVING GROUND, MD 21005

DIRECTOR
US ARMY BALLISTIC RESEARCH
LABORATORY
ATTN DRDAR-TSB-S (STINFO)
ABERDEEN PROVING GROUND, MD 21005

US ARMY ELECTRONICS TECHNOLOGY
& DEVICES LABORATORY
ATTN DELET-DD
FT MONMOUTH, NJ 07703

HQ, USAF/SAMI
WASHINGTON, DC 20330

TELEDYNE BROWN ENGINEERING
CUMMINGS RESEARCH PARK
ATTN DR MELVIN L. PRICE, MS-44
HUNTSVILLE, AL 35807

ENGINEERING SOCIETIES LIBRARY
ATTN ACQUISITIONS DEPARTMENT
345 EAST 47TH ST
NEW YORK, NY 10017

COMMANDER
US ARMY MATERIEL DEVELOPMENT
& READINESS COMMAND
ATTN DRCDE, DIR FOR DEV & ENGR
ATTN DRCNC, NUCLEAR-CHEMICAL OPC
5001 EISENHOWER AVE
ALEXANDRIA, VA 22333

ARGONNE NATIONAL LABORATORY
9700 SOUTH CASS AVE
ARGONNE, IL 60439

BROOKHAVEN NATIONAL LABORATORY
ASSOCIATED UNIVERSITIES, INC
UPTON, LONG ISLAND, NY 11973

US DEPARTMENT OF COMMERCE
ASSISTANT SECRETARY FOR SCIENCE
& TECHNOLOGY
WASHINGTON, DC 20230

DEPT OF ENERGY
ATTN ASST SEC FOR NUCLEAR ENERGY
ATTN DIV OF SPACE NUCLEAR SYSTEMS
ATTN DIV OF REACTOR RES & DEV
WASHINGTON, DC 20585

DEPT OF ENERGY
ALBUQUERQUE OPERATIONS
ATTN DOCUMENT CONTROL FOR WSSB
PO BOX 5400
ALBUQUERQUE, NM 87115

DEPT OF ENERGY
TECHNICAL INFORMATION ORGANIZATION
PO BOX 62
OAK RIDGE, TN 37830

DIRECTOR
ARMED FORCES RADIOBIOLOGY RESEARCH
INSTITUTE
ATTN R. WEISS, CPT
DEFENSE NUCLEAR AGENCY
NATIONAL NAVAL MEDICAL CENTER
BETHESDA, MD 20014

COMMANDER
US ARMAMENT RES & DEV COMMAND
ATTN DRDAR-LCN, NUCLEAR & FUZE DIV
ATTN DRDAR-NC, NUCLEAR/CHEMICAL
SURETY GP
ATTN DRDAR-TSS, STINFO DIV
DOVER, NJ 07801

DIRECTOR
DEFENSE ADVANCED RESEARCH
PROJECTS AGENCY
ATTN DIR, MATERIAL SCIENCES
ATTN TECH INFO OFFICE
ATTN DIR, STRATEGIC TECHNOLOGY
OFFICE
ATTN DIR, TECHNOLOGY
ASSESSMENTS OFFICE
1400 WILSON BLVD
ARLINGTON, VA 22209

DEFENSE COMMUNICATIONS ENGINEERING
CENTER
ATTN CODE R320, C. W. BERGMAN
ATTN CODE R410, JAMES W. MCLEAN

DEFENSE COMMUNICATIONS ENGINEERING
CENTER (Cont'd)
ATTN RES & DEV
1860 WIEHLE AVE
RESTON, VA 22090

DIRECTOR
DEFENSE COMMUNICATIONS AGENCY
ATTN CODE 930, MONTE I. BURGETT, JR
ATTN TECH LIBRARY
WASHINGTON, DC 20305

DIRECTOR
DEFENSE INTELLIGENCE AGENCY
ATTN DS-4A2
WASHINGTON, DC 20301

DIRECTOR
DEFENSE NUCLEAR AGENCY
ATTN RAEV (4 COPIES)
ATTN TITL, TECH LIBRARY
WASHINGTON, DC 20305

DIRECTOR
DEFENSE COMMUNICATIONS AGENCY
NATIONAL MILITARY COMMAND
SYSTEM SUPPORT CENTER
ATTN TECHNICAL DIRECTOR (B102)
WASHINGTON, DC 20305

UNDER SECRETARY OF DEFENSE FOR
RSCH & ENGINEERING
DEPARTMENT OF DEFENSE
ATTN ASST TO SEC/ATOMIC ENERGY
ATTN DEP ASST SEC/ENERGY ENVIRONMENT
& SAFETY
ATTN DEP UNDER SEC/TEST & EVALUATION
ATTN DEP UNDER SEC/RES & ADVANCED
TECH
WASHINGTON, DC 20301

COMMANDER
FIELD COMMAND
DEFENSE NUCLEAR AGENCY
ATTN FCPR
KIRTLAND AFB, NM 87115

DIRECTOR
INTERSERVICE NUCLEAR WEAPONS SCHOOL
ATTN DOCUMENT CONTROL
KIRTLAND AFB, NM 87115

DIRECTOR
JOINT STRATEGIC TARGET PLANNING
STAFF, JCS
ATTN JLTW-2
OFFUTT AFB
OMAHA, NB 68113

GSA/FPA
GS BLDG, 18TH & F STS NW
ATTN EGT
WASHINGTON, DC 20405

CHIEF
LIVERMORE DIVISION, FIELD COMMAND
DNA
LAWRENCE LIVERMORE LABORATORY
ATTN FCPRL
PO BOX 808
LIVERMORE, CA 94550

DIRECTOR
NATIONAL SECURITY AGENCY
ATTN O. O. VAN GUNTEN, R-425
ATTN TDL
FT MEADE, MD 20755

OFFICE OF THE DEPUTY CHIEF OF STAFF
FOR RESEARCH, DEV & ACQUISITION
ATTN DAMA-ARZ-A, DIR OF ARMY RES,
DR M. E. LASSER
ATTN DAMA-ARZ-D, RESEARCH PROGRAMS
ATTN DAMA-RAX, SYS REVIEW &
ANALYSIS OFC
ATTN DAMA-CSS-D, R&D TEAM
WASHINGTON, DC 20310

BALLISTIC MISSILE DEFENSE PROGRAM
MANAGER OFFICE
ATTN TECHNOLOGY DIR
5001 EISENHOWER AVE
ALEXANDRIA, VA 22333

DIRECTOR
SIGNALS WARFARE LAB, VHFS
ATTN DELSW-DT, TAC DATA SYS DIV
WARRENTON, VA 22186

COMMANDER
BMD SYSTEMS COMMAND
PO BOX 1500
ATTN BMDSC-TEN, NOAH J. HURST
ATTN BMDSC-T, TEST & SYS ENGR
SUP DIR
ATTN R. C. WEBB
HUNTSVILLE, AL 35807

COMMANDER
BALLISTIC MISSILE DEFENSE ADVANCED
TECHNOLOGY CENTER
PO BOX 1500
ATTN DIRECTOR, ATC-X
ATTN TECH LIB
HUNTSVILLE, AL 35807

COMMANDER
US ARMY COMMUNICATIONS COMMAND
ATTN TECH LIB
FT HUACHUCA, AZ 85613

COMMANDER
US ARMY COMPUTER SYS COMMAND
ATTN TECH LIB
FT MONMOUTH, VA 22060

PROJECT MANAGER, PATRIOT
AIR DEFENSE MISSILE SYS
REDSTONE ARSENAL, AL 35809

US ARMY MISSILE LABORATORY
US ARMY MISSILE COMMAND
ATTN DRSMI-RF, ADV SYS CONCEPTS OFC
ATTN DRSMI-RG, GUIDANCE & CONTROL
ATTN DRSMI-RE, ADVANCED SENSORS DIR
REDSTONE ARSENAL, AL 35809

DIRECTOR
NIGHT VISION & ELECTRO-OPTICS
LABORATORY
ATTN CPT ALLAN S. PARKER
ATTN TECHNICAL LIBRARY
ATTN DELNV-TMS-IO, INFORMATION OFC
ATTN DELNV-SI, ELECTRONICS TEAM
FT BELVOIR, VA 22060

COMMANDER
REDSTONE SCIENTIFIC INFORMATION CTR
US ARMY MISSILE COMMAND
ATTN CHIEF, DOCUMENTS
REDSTONE ARSENAL, AL 35809

SECRETARY OF THE ARMY
ATTN OUSA OR DANIEL WILLARD
WASHINGTON, DC 20310

ASSISTANT SECRETARY OF THE ARMY
RES, DIV, & ACQ
ATTN DEP FOR SCIENCE & TECHNOLOGY
WASHINGTON, DC 20310

COMMANDER
TRASANA
ATTN ATAA-EAC, FRANCIS N. WINANS
WHITE SANDS MISSILE RANGE, NM 88002

DIRECTOR
US ARMY BALLISTIC RESEARCH
LABORATORY
ATTN DRXBR-BVL, DAVID L. RIGOTTI
ATTN DRXBR-X, JULIUS J. MESZAROS
ATTN DRXBR-AM, W. R. VANANTWERP
ATTN DRXBR-VL, JOHN W. KINCH
ATTN DRXBR-VL, ROBERT L. HARRISON
ABERDEEN PROVING GROUND, MD 21005

CHIEF
US ARMY COMMUNICATIONS SYSTEMS
AGENCY
ATTN SCCM-AD-SV (LIBRARY)
FT MONMOUTH, NJ 07703

DIRECTOR
US ARMY ELECTRONICS TECHNOLOGY
& DEVICES LAB, ERADCOM
ATTN DELET-ER,
DR STANLEY KRONENBERG
ATTN DELET-I, MICROELECTRONICS DIV
ATTN DELET-IA, DR E. T. HUNTER
ATTN DELET-ER-S, DR R. LUX
ATTN DELET-E, ELECTRONIC MAT RES DIV
FT MONMOUTH, NJ 07703

COMMANDER
ATMOSPHERIC SCIENCES LABORATORY,
ERADCOM
ATTN TECHNICAL LIBRARY
WHITE SANDS MISSILE RANGE, NM 88002

DIRECTOR
US ARMY ELECTRONIC WARFARE
LABORATORY, ERADCOM
ATTN DELEW-DI, INFORMATION SYS
OFFICE
ATTN DELEW-V, ELECTROMAGNETIC
VULNERABILITY & ECCM DIV
FT MONMOUTH, NJ 07703

COMMANDER
OFFICE OF MISSILE ELECTRONIC WARFARE
ATTN TECH & ADV CONCEPTS DIV
WHITE SANDS MISSILE RANGE, NM 88002

COMMANDER
ERADCOM TECHNICAL SUPPORT ACTIVITY
TECHNICAL LIBRARY DIV
ATTN DELSO-L
FT MONMOUTH, NJ 07703

COMMANDANT
US ARMY ENGINEER SCHOOL
FT BELVOIR, VA 22060

COMMANDANT
US ARMY FIELD ARTILLERY SCHOOL
ATTN ATSFA-CTD-ME, HARLEY MOBERG
FT SILL, OK 73503

COMMANDER
US ARMY MISSILE COMMAND
ATTN DRCPM-PE-EA, WALLACE O. WAGNER
ATTN DRSMI-RGP, VICTOR W. RUWE
ATTN DRCPM-MDTI, CPT JOE A. SIMS
ATTN DRCPM-LCEX, HOWARD H. HENRIKSEN

COMMANDER
US ARMY MISSILE COMMAND (Cont'd)
ATTN DRSMI-RGP, HUGH GREEN
ATTN ARMY MISSILE RDE LAB
ATTN TECH LIB
REDSTONE ARSENAL
HUNTSVILLE, AL 35809

COMMANDER
US ARMY MOBILITY EQUIP R&D COMMAND
ATTN JOHN W. BOND, JR
ATTN DRDME, VR, RADIATION
RESEARCH GRP
FT BELVOIR, VA 22060

CHIEF
US ARMY NUC & CHEMICAL AGENCY
ATTN MAJ SIDNEY W. WINSLOW
FT BELVOIR, VA 22060

COMMANDER
US ARMY NUCLEAR & CHEMICAL AGENCY
ATTN ATCN-W, LTC LEONARD A. SLUGA
ATTN ATCN-W WEAPONS EFFECTS DIV
ATTN TECH LIB
7500 BACKLICK RD
BLDG 2073
SPRINGFIELD, VA 22150

COMMANDER
US ARMY TANK-AUTOMOTIVE COMMAND
ATTN DRCPM-GCM-SW, LYLE A. WOLCOTT
WARREN, MI 48090

COMMANDER
US ARMY TEST & EVALUATION COMMAND
ATTN DRSTE-EO, R. I. KOLCHIN
ATTN DRSTE-CM-F, R. R. GALASSO
ATTN DRSTE-TO-O, TEST OPERATIONS DIV
ABERDEEN PROVING GROUND, MD 21005

COMMANDER
WHITE SANDS MISSILE RANGE
ATTN STEWS-TE-NT,
MR MARVIN P. SQUIRES
WHITE SANDS MISSILE RANGE, NM 88002

COMMANDER
EDGEWOOD ARSENAL
ATTN DRDAR-CLS, CHEMICAL SURETY OFC
ATTN DRDAR-CLT, ENVIRONMENTAL
TECHNOLOGY DIV
ATTN DRDAR-CLB, RESEARCH DIV
ABERDEEN PROVING GROUND, MD 21005

OFFICE OF RESEARCH, DEVELOPMENT,
TEST & EVALUATION
DEPT OF THE NAVY
ATTN OP-987, R&D PLANS
WASHINGTON, DC 20360

US NAVAL ACADEMY
ENGINEERING DEPT
ATTN LIBRARY
ANNAPOLIS, MD 21402

COMMANDER
NAVAL AIR SYSTEMS COMMAND HQ
ATTN TECHNICAL LIBRARY
DEPT OF THE NAVY
WASHINGTON, DC 20360

COMMANDER
NAVAL OCEAN SYSTEMS CENTER
ATTN CODE 6400, TECH INFO DIV
SAN DIEGO, CA 92152

SUPERINTENDENT
NAVAL POSTGRADUATE SCHOOL
ATTN LIBRARY, CODE 2124
MONTEREY, CA 93940

CHIEF OF NAVAL RESEARCH
NAVY DEPARTMENT
ATTN CODE 427
ATTN CODE 421, DORAN W. PADGETT
ATTN TECHNICAL LIBRARY
ARLINGTON, VA 22217

COMMANDING OFFICER
NAVAL AVIONICS FACILITY
ATTN BRANCH 942, D. J. REPASS
21ST & ARLINGTON AVE
INDIANAPOLIS, IN 46218

COMMANDER
HQ, NAVAL ELECTRONIC SYSTEMS COMMAND
ATTN ELEX 05323,
CLEVELAND F. WATKINS
ATTN CODE 5032, CHARLES W. NEILL
ATTN CODE 504511, CHARLES R. SUMAN
WASHINGTON, DC 20360

COMMANDING OFFICER
NAVAL INTELLIGENCE SUPPORT CENTER
ATTN NISC-45
ATTN P. ALEXANDER
4301 SUITLAND ROAD, BLDG 5
WASHINGTON, DC 20390

DIRECTOR
NAVAL RESEARCH LABORATORY
ATTN CODE 6601, CHARLES GUENZER
ATTN CODE 6601, E. WOLICKI
ATTN CODE 6631, JAMES C. RITTER
ATTN CODE 4004, EMANUAL L. BRANCATO
ATTN CODE 2627, DORIS R. FOLEN
ATTN CODE 7701, JACK D. BROWN
ATTN CODE 6816
ATTN CODE 5210, JOHN E. DAVEY

DIRECTOR
NAVAL RESEARCH LABORATORY (Cont'd)
ATTN CODE 6627, C. GUENEER
ATTN CODE 6440, GEORGE SIGEL
ATTN CODE 2620, LIBRARY
ATTN CODE 4000, RESEARCH DEPT
ATTN CODE 6620, RADIATION EFFECTS
WASHINGTON, DC 20375

COMMANDER
NAVAL SEA SYSTEMS COMMAND
NAVY DEPARTMENT
ATTN SEA-9931, RILEY B. LANE
ATTN SEA-9931, SAMUEL A. BARHAM
ATTN SEA-09G32, TECH LIB
WASHINGTON, DC 20362

NAVAL SHIP ENGINEERING CENTER
DEPT OF THE NAVY
ATTN CODE 6174D2, EDWARD F. DUFFY
WASHINGTON, DC 20362

COMMANDER
NAVAL SURFACE WEAPONS CENTER
ATTN CODE WX21, TECH LIB
ATTN CODE WA501, NAVY NUC PRGMS OFC
ATTN CODE WA50
ATTN CODE WA52, R. A. SMITH
ATTN CODE WR, RESEARCH &
TECHNOLOGY DEPT
WHITE OAK, SILVER SPRING, MD 20910

COMMANDER
NAVAL SURFACE WEAPONS CENTER
ATTN WILLIAM H. HOLT
ATTN DX-21, LIBRARY DIV
DAHLGREN LABORATORY
DAHLGREN, VA 22448

COMMANDER
NAVAL WEAPONS CENTER
ATTN CODE 533, TECHNICAL LIBRARY
CHINA LAKE, CA 93555

COMMANDING OFFICER
NAVAL WEAPONS EVALUATION FACILITY
ATTN CODE ATG, MR STANLEY
KIRTLAND AIR FORCE BASE
ALBUQUERQUE, NM 87117

COMMANDING OFFICER
NAVAL WEAPONS SUPPORT CENTER
ATTN CODE 7024, JAMES RAMSEY
ATTN CODE 70242, JOSEPH A. MUNARIN
CRANE, IN 47522

COMMANDING OFFICER
NUCLEAR WEAPONS TRAINING
CENTER PACIFIC
ATTN CODE 50
NAVAL AIR STATION, NORTH ISLAND
SAN DIEGO, CA 92135

DIRECTOR
STRATEGIC SYSTEMS PROJECT OFFICE
ATTN SP2701, JOHN W. PITSENBERGER
ATTN NSP-2342, RICHARD L. COLEMAN
ATTN NSP-27331, PHIL SPECTOR
NAVY DEPARTMENT
WASHINGTON, DC 20376

ASSISTANT SECRETARY OF THE AIR FORCE
(RESEARCH & DEVELOPMENT)
WASHINGTON, DC 20330

DEPUTY CHIEF OF STAFF, RES & DEV
US AIR FORCE
ATTN RDQPN, S/V & NUCLEAR PROG DIV
WASHINGTON, DC 20330

COMMANDER-IN-CHIEF
AEROSPACE DEFENSE COMMAND
ATTN TECHNICAL LIBRARY
ENT AIR FORCE BASE, CO 80912

COMMANDER
AEROSPACE RESEARCH LABORATORIES
ATTN LS, SOLID STATE PHYSICS RES LAB
WRIGHT-PATTERSON AFB, OH 45433

DIRECTOR
AF AVIONICS LABORATORY
ATTN TE, ELECTRONIC TECHNOLOGY DIV
ATTN TER, ELECTRONIC RES BR
ATTN TSR, STINFO BR
ATTN DHE, H. J. HENNECKE
ATTN DHM, C. FRIEND
ATTN DH, LTC MCKENZIE
ATTN AAT, MASON FRIAR
WRIGHT-PATTERSON AFB, OH 45433

COMMANDER
AF CAMBRIDGE RESEARCH LABORATORIES,
AFSC
ATTN LQ, SOLID-STATE SCI LAB
L. G. HANSCOM FIELD
BEDFORD, MA 01730

COMMANDER
AF FLIGHT DYNAMICS LAB
ATTN PTS, SURVIVABILITY/
VULNERABILITY BR
ATTN STS, TECH INFO BR
WRIGHT-PATTERSON AFB, OH 45433

AF GEOPHYSICS LABORATORY, AFSC
ATTN J. EMERY CORMIER
ATTN LGD-STOP 30, FREEMAN SHEPHERD
ATTN LQR, EDWARD A. BURKE
HANSCOM AFB, MA 01731

AF INSTITUTE OF TECHNOLOGY, AU
ATTN ENP, CHARLES J. BRIDGMAN
WRIGHT-PATTERSON AFB, OH 45433

AF WEAPONS LABORATORY, AFSC
ATTN ELA
ATTN SAB
ATTN DEX
ATTN ELS
ATTN NTS
ATTN ELXT
ATTN SE, NUCLEAR SYS DIV
ATTN DYC
ATTN NTYC (J. MULLIS)
KIRTLAND AFB, NM 87117

AFTAC
ATTN TFS, MAJ MARION F. SCHNEIDER
ATTN TAE
PARTICK AFB, FL 32925

COMMANDER
ASD
ATTN ASD/ENESS, PETER T. MARTH
ATTN ASD-YH-EX, LTC ROBERT LEVERETTE
ATTN ENACC, ROBERT L. FISH
WRIGHT-PATTERSON AFB, OH 45433

HEADQUARTERS
ELECTRONIC SYSTEMS DIVISION, (AFSC)
ATTN YWEI
ATTN YSEV
HANSCOM AFB, MA 01731

COMMANDER
FOREIGN TECHNOLOGY DIVISION, AFSC
ATTN ETET, CPT RICHARD C. HUSEMANN
WRIGHT-PATTERSON AFB, OH 45433

COMMANDER
ROME AIR DEVELOPMENT CENTER, AFSC
ATTN RBRAC, I. L. KRULAC
ATTN RBRP, CLYDE LANE
ATTN TUT, TEST & EVAL BR
ATTN TIL, TECHNICAL LIBRARY
GRIFFISS AFB, NY 13440

COMMANDER
ROME AIR DEVELOPMENT CENTER, AFSC
ATTN ET, R. BUCHANAN
ATTN ESR, P. VAIL, MS-64
HANSCOM AFB, MA 01731

DIRECTOR
AF OFFICE OF SCIENTITIC RESEARCH
ATTN NE, DIR OF ELECTRONIC
& SOLID STATE SCI
BOLLING AFB, DC 20332

COMMANDER
SPACE DIV, AFSC
PO BOX 92960
WORLDWAY POSTAL CENTER
ATTN RS, DEP FOR REENTRY SYS
ATTN LV, DEP FOR LAUNCH VEHICLES
ATTN SK, DEP FOR COMM SYS
ATTN SD/YLX
ATTN DYS, MAJ LARRY A. DARDA
ATTN IND, I. J. JUDY
ATTN LTC KENNETH L. GILBERT
ATTN RSMG, CPT COLLIER
ATTN SZJ, CPT JOHN H. SALCH
LOS ANGELES, CA 90009

COMMANDER
AF SPECIAL WEAPONS CENTEF (OAS)
ATTN TE, TEST & EVAL SYS PROG OFC
KIRTLAND AFB, NM 87117

COMMANDER
HQ AIR FORCE SYSTEMS COMMAND
ATTN TECHNICAL LIBRARY
ANDREWS AFB
WASHINGTON, DC 20331

BMO
ATTN MNNG, CPT DAVID J. STROBEL
ATTN MNNH
NORTON AFB, CA 92409

COMMANDER-IN-CHIEF
STRATEGIC AIR COMMAND
ATTN NRI-STINFO LIBRARY
ATTN XPFS, MAJ BRIAN STEPHAN
OFFUTT AFB, NB 68113

UNIVERSITY OF CALIFORNIA
LAWRENCE LIVERMORE LABORATORY
PO BOX 808
ATTN DONALD J. MEEKER, L-545
ATTN DALE E. MILLER, L-156
ATTN JOSEPH E. KELLER, JR, L-125
ATTN RONALD L. OTT, L-531
ATTN HANS KRUGER, L-96
ATTN LAWRENCE CLELAND, L-156
ATTN FREDERICK R. KOVAR, L-31
ATTN TECH INFO DEPT, L-3
LIVERMORE, CA 94550

LOS ALAMOS SCIENTIFIC LABORATORY
PO BOX 1663
ATTN MARVIN M. HOFFMAN
ATTN J. ARTHUR FREED
ATTN BRUCE W. NOEL
LOS ALAMOS, NM 87544

SANDIA LABORATORIES
LIVERMORE LABORATORY
PO BOX 969
ATTN THEODORE A. DELLIN
LIVERMORE, CA 94550

SANDIA NATIONAL LABORATORIES
PO BOX 5800
ATTN 3141 SANDIA RPT COLL
ATTN ORG 2110, J. A. HOOD
ATTN 5220, JACK V. WALKER
ATTN ORG 1933, F. N. COPPAGE
ATTN DIV 5231, JAMES H. RENKEN
ATTN ORG 2140, R. GREGORY
ATTN W. DAWES
ATTN DIV 2123, W. H. BURNETT
ATTN DIV 4232, W. BEEZHOLD
ALBUQUERQUE, NM 87185

ADMINISTRATOR
NASA HEADQUARTERS
ATTN OFC OF AERONAUTICS
& SPACE TECHNOLOGY
WASHINGTON, DC 20546

AMES RESEARCH CENTER
NASA
ATTN DIR OF RESEARCH SUPPORT
MOFFETT FIELD, CA 94035

DIRECTOR
NASA
GODDARD SPACE FLIGHT CENTER
ATTN 250, TECH INFO DIV
GREENBELT, MD 20771

DIRECTOR
NASA
HUGH L. DRYDEN FLIGHT RESEARCH
CENTER
ATTN TECHNICAL LIBRARY
EDWARDS, CA 93523

DIRECTOR
NASA
ATTN TECHNICAL LIBRARY
JOHN F. KENNEDY SPACE CENTER,
FL 32899

DIRECTOR
NASA
LEWIS RESEARCH CENTER
ATTN TECHNICAL LIBRARY
CLEVELAND, OH 44135

JET PROPULSION LABORATORY
CALIFORNIA INSTITUTE OF TECHNOLOGY
ATTN J. W. WINSLOW, 157-103
ATTN TECHNICAL LIBRARY
ATTN D. J. NICHOLS, T-1180
4800 OAK GROVE DRIVE
PASADENA, CA 91103

OAK RIDGE NATIONAL LABORATORIES
PO BOX X
ATTN J. C. ASHLEY
OAK RIDGE, TN 37830

DIRECTOR
NASA
LANGLEY RESEARCH CENTER
ATTN TECHNICAL LIBRARY
ATTN INSTR RES DIV
HAMPTON, VA 23665

DIRECTOR
NASA
GEORGE C. MARSHALL SPACE FLIGHT
CENTER
ATTN EA, SCI & ENGR
ATTN EC, ELECTRONICS & CONTROL LAB
ATTN EC-21, GUIDANCE, CONTROL
& INSTR DIV
ATTN EC-41, ELECTRONICS DEV DIV
ATTN ES-21, RADIATION & LOW TEMP SCI
ATTN ES-31, PHYSICS & INSTR DIV
MARSHALL SPACE FLIGHT CENTER,
AL 35812

CENTRAL INTELLIGENCE AGENCY
ATTN RD/SI, RM 5G48, HQ BLDG
ATTN ALICE A. PADGETT
WASHINGTON, DC 20505

DEPARTMENT OF COMMERCE
NATIONAL BUREAU OF STANDARDS
ATTN APPL RAD DIV,
ROBERT C. PLACIOUS
ATTN JUDSON C. FRENCH
WASHINGTON, DC 20230

AEROJET ELECTRO-SYSTEMS CO DIV
AEROJET-GENERAL CORP
PO BOX 296
ATTN THOMAS D. HANSCOME, B170/D6711
AZUSA, CA 91702

AEROSPACE CORP
PO BOX 92957
ATTN IRVING M. GARFUNKEL
ATTN JULIAN REIHEIMER
ATTN LIBRARY
ATTN WILLIAM W. WILLIS
ATTN S. P. BOWER
ATTN JOHN DITRE
ATTN L. W. AUKERMAN
LOS ANGELES, CA 90009

ANALOG TECHNOLOGY CORP
ATTN JOHN JOSEPH BAUM
15859 EAST EDNA PLACE
IRWINDALE, CA 91706

ANALYTICAL SYSTEMS ENGINEERING CORP
5 OLD CONCORD RD
BURLINGTON, MA 01803

AVCO RESEARCH & SYSTEMS GROUP
ATTN RESEARCH LIB, A830, RM 7201
201 LOWELL ST
WILMINGTON, MA 01887

BELL LABORATORIES
ATTN RICHARD B. FAIR
READING, PA 19604

BDM CORP, THE
ATTN T. H. NEIGHBORS
7915 JONES BR DRIVE
MCLEAN, VA 22102

BDM CORP, THE
PO BOX 9274
ATTN D. R. ALEXANDER
ALBUQUERQUE INTERNATIONAL
ALBUQUERQUE, NM 87119

BELL LABS
ATTN D. S. YANEY
ALLENTOWN, PA 18100

BENDIX CORP, THE
COMMUNICATION DIVISION
ATTN DOCUMENT CONTROL
EAST JOPPA ROAD-TOWSON
BALTIMORE, MD 21204

BENDIX CORP, THE
RESEARCH LABORATORIES DIV
ATTN MGR PRGM DEV, DONALD J. NIEHAUS
ATTN MAX FRANK
BENDIX CENTER
SOUTHFIELD, MI 48075

BOEING COMPANY, THE
PO BOX 3707
ATTN HOWARD W. WICKLEIN, MS 17-11
ATTN DAVID DYE, MS 87-75
ATTN AEROSPACE LIBRARY
ATTN ROBERT S. CALDWELL, 2R-00
SEATTLE, WA 98124

CALIFORNIA INSTITUTE OF TECHNOLOGY
JET PROPULSION LABORATORY
ATTN J. BRYDEN
ATTN A. G. STANLEY
ATTN J. MASERJIAN
4800 OAK GROVE DRIVE
PASADENA, CA 91103

CALSPAN CORP
PO BOX 400
ATTN RAY MISSERT
BUFFALO, NY 14225

CHARLES STARK DRAPER LABORATORY, INC
ATTN KENNETH FERTIG
ATTN PAUL R. KELLY
ATTN RICHARD G. HALTMAIER
555 TECHNOLOGY SQUARE
CAMBRIDGE, MA 02139

CINCINNATI ELECTRONICS CORP
ATTN C. R. STUMP
ATTN LOIS HAMMOND
2630 GLENDALE-MILFORD ROAD
CINCINNATI, OH 45241

COMPUTER SCIENCES CORP
ATTN TECHNICAL LIBRARY
1400 SAN MATEO BLVD, SE
ALBUQUERQUE, NM 87108

CUTLER-HAMMER, INC
AIL DIVISION
ATTN CENTRAL TECH FILES, ANN ANTHONY
COMAC ROAD
DEER PARK, NY 11729

DIKEWOOD CORP, THE
ATTN L. WAYNE DAVIS
1613 UNIVERSITY BLVD, NE
ALBUQUERQUE, NM 87102

E-SYSTEMS, INC
GREENVILLE DIVISION
PO BOX 1056
ATTN LIRARY 8-50100
GREENVILLE, TX 75401

EFFECTS TECHNOLOGY, INC
ATTN EDWARD JOHN STEELE
5383 HOLLISTER AVE
SANTA BARBARA, CA 93111

EXPERIMENTAL & MATHEMATICAL
PHYSICS CONSULTANTS
PO BOX 66331
LOS ANGELES, CA 90066

FAIRCHILD CAMERA & INSTRUMENT
CORP
ATTN 2-233, MR DAVID K. MEYERS
464 ELLIS ST
MOUNTAIN VIEW, CA 94040

FAIRCHILD INDUSTRIES, INC
SHERMAN FAIRCHILD TECHNOLOGY CENTER
ATTN MGR CONFIG DATA & STANDARDS
20301 CENTURY BOULEVARD
GERMANTOWN, MD 20767

FAIRCHILD-WESTON
ATTN HENRY SADOWSKI
300 ROBBINS LA
SYOSSET, NY 11791

FLORIDA, UNIVERSITY OF
AN INSTITUTION OF EDUCATION
PO BOX 284
ATTN PATRICIA B. RAMBO
ATTN D. P. KENNEDY
GAINESVILLE, FL 32601

FORD AEROSPACE & COMMUNICATIONS CORP
ATTN EDWARD R. HAHN, MS-X22
3939 FABIAN WAY
PALO ALTO, CA 94303

FORD AEROSPACE & COMMUNICATIONS
OPERATIONS
ATTN KEN C. ATTINGER
ATTN E. R. PONCELET, JR
ATTN TECH INFO SECTION
FORD & JAMBOREE ROADS
NEWPORT BEACH, CA 92663

FRANKLIN INSTITUTE, THE
ATTN RAMIE H. THOMPSON
20TH ST & PARKWAY
PHILADELPHIA, PA 19103

GARRETT CORP
ATTN ROBERT E. WEIR, DEPT 93-9
2525 W 190TH ST
TORRENCE, CA 90509

GENERAL ELECTRIC COMPANY
SPACE DIVISION
VALLEY FORGE SPACE CENTER
GODDARD BLVD KING OF PRUSSIA
PO BOX 8555
ATTN KOJI ITO
ATTN LARRY I. CHASEN
ATTN JOSEPH C. PEDEN, CCF 8301
ATTN JOHN L. ANDREWS
PHILADELPHIA, PA 19101

GENERAL ELECTRIC COMPANY
RE-ENTRY & ENVIRONMENTAL SYSTEMS DIV
PO BOX 7722
ATTN ROBERT V. BENEDICT
ATTN R. H. CASEY
3198 CHESTNUT ST
PHILADELPHIA, PA 19101

GENERAL ELECTRIC COMPANY
ORDNANCE SYSTEMS
ATTN JOSEPH J. REIDL
100 PLASTICS AVE
PITTSFIELD, MA 01201

GENERAL ELECTRIC COMPANY
ATTN L. J. RAGONESE
BLDG 3, RM 116
SYRACUSE, NY 13221

GENERAL ELECTRIC COMPANY
AIRCRAFT ENGINE GROUP
ATTN JOHN A. ELLERHORST, E2
EVENDALE PLANT, INT HWY 75 S
CINCINNATI, OH 45215

GENERAL ELECTRIC COMPANY
AEROSPACE ELECTRONICS SYSTEMS
ATTN CHARLES M. HEWISON, DROP 624
FRENCH ROAD
UTICA, NY 13503

GENERAL ELECTRIC COMPANY
PO BOX 5000
ATTN D. W. PEPIN, DROP 160
BINGHAMTON, NY 13902

GENERAL RESEARCH CORP
ATTN ROBERT D. HILL
PO BOX 6770
SANTA BARBARA, CA 93111

GEORGIA INSTITUTE OF TECHNOLOGY
GEORGIA TECH RESEARCH INSTITUTE
ATTN R. CURRY
ATLANTA, GA 30332

GRUMMAN AEROSPACE CORP
ATTN JERRY ROGERS, DEPT 533
SOUTH OYSTER BAY ROAD
BETHPAGE, NY 11714

GTE SYLVANIA, INC
ELECTRONICS SYSTEMS GRP-EASTERN DIV
ATTN CHARLES A. THORN HILL, LIBRARIAN
ATTN LEONARD L. BLAISDELL
ATTN JAMES A. WALDON
77 A ST
NEEDHAM HEIGHTS, MA 02194

GTE SYLVANIA, INC
ATTN CHARLES H. RAMSBOTTOM
ATTN HERBERT A. ULLMAN
ATTN H & V GROUP
ATTN PAUL B. FREDERICKSON
189 B ST
NEEDHAM HEIGHTS, MA 02194

GULTON INDUSTRIES, INC
ENGINEERED MAGNETICS DIVISION
ATTN ENGNMAGNETICS DIV
13041 CERISE AVE
HAWTHORNE, CA 90250

HARRIS CORP
HARRIS SEMICONDUCTOR DIVISION
PO BOX 883
ATTN C. F. DAVIS, MS 17-220
ATTN T. CLARK, MS 4040
ATTN WAYNE E. ABARE, MS 16-111
MELBOURNE, FL 32901

HAZELTINE CORP
ATTN TECH INFO CTR, M. WAITE
PULASKI ROAD
GREENLAWN, NY 11740

HONEYWELL, INC
GOVERNMENT & AERONAUTICAL
PRODUCTS DIVISION
ATTN RONALD R. JOHNSON, A1622
ATTN R. J. KELL, MS S2572
2600 RIDGEWAY PARKWAY
MINNEAPOLIS, MN 55413

HONEYWELL, INC
AEROSPACE DIVISION
ATTN HARRISON H. NOBLE, MS 725-5A
ATTN MS 725-J, STACEY H. GRAFF
13350 US HIGHWAY 19
ST PETERSBURG, FL 33733

HONEYWELL, INC
RADIATION CENTER
ATTN TECHNICAL LIBRARY
2 FORBES ROAD
LEXINGTON, MA 02173

HUGHES AIRCRAFT COMPANY
ATTN M.S. D157, KEN WALKER
ATTN B. W. CAMPBELL, M.S. 6-E110
ATTN DAN BINDER, MS 6-D147
ATTN JOHN B. SINGLETARY, MS 6-D113
CENTINELLA & TEALE
CULVER CITY, CA 90230

HUGHES AIRCRAFT COMPANY
SPACE SYSTEMS DIVISION
PO BOX 92919
ATTN WILLIAM W. SCOTT, MS A1080
ATTN EDWARD C. SMITH, MS A620
LOS ANGELES, CA 90009

IBM CORP
THOMAS WATSON RESEARCH CENTER
PO BOX 218
ATTN JOHN AITKEN
ATTN ROBERT DENNARD
YORKTOWN HEIGHTS, NY 10598

IBM CORP
FEDERAL SYSTEMS DIVISION
ATTN FRED TIETZE
MANASSAS, VA 22110

IBM CORP
ATTN HARRY W. MATHERS, DEPT M41
ATTN FRANK FRANKOVSKY
ROUTE 17C
OWEGO, NY 13827

INTEL CORP
ATTN TIM MAY
3585 SW 198TH AVE
ALOHA, OR 97005

INTL TEL & TELEGRAPH CORP
ATTN ALEXANDER T. RICHARDSON
500 WASHINGTON AVE
NUTLEY, NJ 07110

ION PHYSICS CORP
ATTN ROBERT D. EVANS
SOUTH BEDFORD ST
BURLINGTON, MA 01803

IRT CORP
PO BOX 81087
ATTN LEO D. COTTER
ATTN RALPH H. STAHL
ATTN JAMES A. NABER
ATTN R. L. MERTZ
ATTN MARION A. ROSE
ATTN MDC
SAN DIEGO, CA 92138

JAYCOR
ATTN ROBERT SULLIVAN
ATTN CATHERINE TURESKO
205 S. WHITING ST, SUITE 500
ALEXANDRIA, VA 22304

JOHNS HOPKINS UNIVERSITY
APPLIED PHYSICS LABORATORY
ATTN PETER E. PARTRIDGE
JOHNS HOPKINS ROAD
LAUREL, MD 20810

KAMAN SCIENCES CORP
PO BOX 7463
ATTN DONALD H. BRYCE
ATTN ALBERT P. BRIDGES
ATTN WALTER E. WARE
ATTN JOHN R. HOFFMAN
ATTN JERRY I. LUBELL
COLORADO SPRINGS, CO 80933

KAMAN TEMPO
ATTN WILLIAM ALFONTE
2560 HUNTINGTON AVE
SUITE 506
ALEXANDRIA, VA 22303

LITTON SYSTEMS, INC
GUIDANCE & CONTROL SYSTEMS DIVISION
ATTN VAL J. ASHBY, MS 67
ATTN JOHN P. RETZLER
5500 CHANOGA AVE
WOODLAND HILLS, CA 91364

LITTON SYSTEMS, INC
ELECTRON TUBE DIVISION
ATTN FRANK J. MCCARTHY
1035 WESTMINISTER DRIVE
WILLIAMSPORT, PA 17701

LOCKHEED MISSILES & SPACE
COMPANY, INC
PO BOX 504
ATTN G. F. HEATH, D/81-14
ATTN BENJAMIN T. KIMURA, DEPT 81-14
ATTN EDWIN A. SMITH, DEPT 85-85
ATTN L. ROSSI, DEPT 81-64
ATTN G. H. MORRIS, 81-01
ATTN DEPT 85-85, SAMUEL I. TAIMUTY
SUNNYVALE, CA 94086

LOCKHEED MISSILES & SPACE COMPANY
ATTN TECH INFO CTR D/COLL
3251 HANOVER ST
PALO ALTO, CA 94304

LINCOLN LABORATORY
BOX 73
ATTN LEONA LOUGHLIN, LIBRARIAN,
A-082
LEXINGTON, MA 02173

MARTIN MARIETTA AEROSPACE
ORLANDO DIVISION
PO BOX 5837
ATTN MONA C. GRIFFITH, LIB MP-30
ATTN WILLIAM W. MRAS, MP-413
ATTN JACK M. ASHFORD, MP-537
ORLANDO, FL 32855

MARTIN MARIETTA CORP
DENVER DIVISION
PO BOX 179
ATTN RESEARCH LIB, 6617, J. R. MCKEE
ATTN PAUL G. KASE, MAIL 8203
ATTN BEN T. GRAHAM, MS PO-454
DENVER, CO 80201

MCDONNELL DOUGLAS CORP
PO BOX 516
ATTN BOB KLOSTER, DE451/19
ATTN TECHNICAL LIBRARY
ST LOUIS, MO 63166

MCDONNELL DOUGLAS CORP
ATTN STANLEY SCHNEIDER
5301 BOLSA AVE
HUNTINGTON BEACH, CA 92647

MCDONNELL DOUGLAS CORP
ATTN TECHNICAL LIBRARY, C1-290/36-84
3855 LAKEWOOD BOULEVARD
LONG BEACH, CA 90846

MISSION RESEARCH CORP
PO DRAWER 719
ATTN WILLIAM C. HART
SANTA BARBARA, CA 93102

MISSION RESEARCH CORP-SAN DIEGO
PO BOX 1209
ATTN V. A. J. VAN LINT
ATTN ROBERT BERGER
ATTN J. P. RAYMOND
LA JOLLA, CA 92038

MITRE CORP, THE
PO BOX 208
ATTN LIBRARY
ATTN M. F. FITZGERALD
BEDFORD, MA 01730

NATIONAL ACADEMY OF SCIENCES
ATTN DR R. S. SHANE,
NAT MATERIALS ADVISORY BOARD
2101 CONSTITUTION AVE, NW
WASHINGTON, DC 20418

NEW MEXICO, UNIVERSITY OF
DEPT OF CAMPUS SECURITY & POLICE
ATTN W. W. GRANNEMANN
1821 ROMA, NE
ALBUQUERQUE, NM 87106

NEW MEXICO, UNIVERSITY OF
ELECTRICAL ENGINEERING
& COMPUTER SCIENCE DEPT
ATTN HAROLD SOUTHWARE
ALBUQUERQUE, NM 87131

NORDEN SYSTEMS
ATTN DENIS LONGO
NORDON PLACE
NORWALK, CT 06856

NORTHROP CORP
ELECTRONIC DIVISION
ATTN BOYCE T. AHLPORT
ATTN JOSEPH D. RUSSO
ATTN GEORGE H. TOWNER
2301 W 120TH ST
HAWTHORNE, CA 90250

NORTHROP RESEARCH & TECHNOLOGY
CENTER
ATTN DAVID N. POCOCK
ATTN ORLIE L. CURTIS
ONE RESEARCH PARK
PALOS VERDES PENN, CA 90274

PALISADES INST FOR RSCH SERVICES, INC
ATTN RECORDS SUPERVISOR
201 VARICK ST
NEW YORK, NY 10014

PHYSICS INTERNATIONAL COMPANY
ATTN CHARLES H. STALLINGS
ATTN JOHN H. HUNTINGTON
2700 MERCED ST
SAN LEANDRO, CA 94577

R&D ASSOCIATES
PO BOX 9695
ATTN S. CLAY ROGERS
MARINA DEL REY, CA 90291

RAYTHEON COMPANY
ATTN GAJANAN H. JOSHI, RADAR SYS LAB
HARTWELL ROAD
BEDFORD, MA 01730

RAYTHEON COMPANY
ATTN HAROLD L. FLESCHER
528 BOSTON POST RD
SUDBURY, MA 01776

RCA CORP
GOVERNMENT & COMMERCIAL SYSTEMS
ASTRO ELECTRONICS DIVISION
PO BOX 800, LOCUST CORNER
PRINCETON, NJ 08540

RCA CORP
DAVID SARNOFF RESEARCH CENTER
ATTN GARY W. HUGHES
ATTN GEORGE J. BRUCKER
W. WINDSOR TOWNSHIP
201 WASHINGTON ROAD, PO BOX 432
PRINCETON, NJ 08540

RCA CORP
CAMDEN COMPLEX
ATTN E. VAN KEUREN, 13-5-2
FRONT & COOPER STS
CAMDEN, NJ 08012

RENSSELAER POLYTECHNIC INSTITUTE
PO BOX 965
ATTN RONALD J. GUTMANN
TROY, NY 12181

RESEARCH TRIANGLE INSTITUTE
PO BOX 12194
ATTN SEC OFFICER FOR
ENG DIV, MAYRANT SIMONS, JR
RESEARCH TRIANGLE PARK, NC 27709

ROCKWELL INTERNATIONAL CORP
ATTN M. J. MCNUTT, MC HA10
ATTN J. C. PICKEL, BB01
ATTN K. F. HULL
ATTN JAMES E. BELL, HA10
ATTN GEORGE C. MESSENGER, FB61
3370 MIROLOMA AVE
ANAHEIM, CA 92803

ROCKWELL INTERNATIONAL CORP
ATTN T. B. YATES
5701 WEST IMPERIAL HIGHWAY
LOS ANGELES, CA 90009

ROCKWELL INTERNATIONAL CORP
ELECTRONICS OPERATIONS
COLLINS RADIO GROUP
ATTN ALAN A. LANGENFELD
ATTN DENNIS SUTHERLAND
ATTN MILDRED A. BLAIR
5225 C. AVE NE
CEDAR RAPIDS, IA 52406

SANDERS ASSOCIATES, INC
ATTN M. L. AITEL, NCA 1-3236
95 CANAL ST
NASHUA, NH 03060

SCIENCE APPLICATIONS, INC
PO BOX 2351
ATTN LARRY SCOTT
ATTN J. ROBERT BEYSTER
LA JOLLA, CA 92038

SCIENCE APPLICATIONS, INC
HUNTSVILLE DIVISION
ATTN NOEL R. BYRN
2109 W. CLINTON AVE
SUITE 700
HUNTSVILLE, AL 35805

SCIENCE APPLICATIONS, INC
ATTN CHARLES STEVENS
5 PALO ALTO SQUARE
PALO ALTO, CA 94304

SCIENCE APPLICATIONS, INC
ATTN WILLIAM L. CHADSEY
8400 WESTPARK DRIVE
MCLEAN, VA 22101

SINGER COMPANY, THE
ATTN IRWIN GOLDMAN, ENG MANAGEMENT
1150 MCBRIDE AVE
LITTLE FALLS, NJ 07424

SINGER COMPANY (DATA SYSTEMS), THE
ATTN TECH INFO CENTER
150 TOTOWA ROAD
WAYNE, NJ 07470

SPERRY RAND CORP
SPERRY FLIGHT SYSTEMS DIVISION
PO BOX 21111
ATTN D. ANDREW SCHOW
PHOENIX, AZ 85036

SPERRY RAND CORP
UNIVAC DIVISION
DEFENSE SYSTEMS DIVISION
PO BOX 3525
ATTN JAMES A. INDA, MS 41T25
ST PAUL, MN 55165

SPERRY RAND CORP
SPERRY DIVISION
SPERRY GYROSCOPE DIVISION
SPERRY SYSTEMS MANAGEMENT DIVISION
ATTN PAUL MARRAFFINO
ATTN CHARLES L. CRAIG EV
MARCUS AVE
GREAT NECK, NY 11020

STANFORD RESEARCH INSTITUTE
3980 EL CAMINO REAL
PALO ALTO, CA 94306

STANFORD RESEARCH INSTITUTE
ATTN MACPHERSON MORGAN
306 WYNN DRIVE, NW
HUNTSVILLE, AL 35805

SUNDSTRAND CORP
ATTN DEPT 763SW, CURTIS WHITE
4751 HARRISON AVE
ROCKFORD, IL 61101

SYSTRON-DONNER CORP
ATTN HAROLD D. MORRIS
ATTN GORDON B. DEAN
3700 SYSTRON DRIVE
CONCORD, CA 94518

TEXAS INSTRUMENTS, INC
PO BOX 60151
ATTN DONALD J. MANUS, MS 72
DALLAS, TX 75265

TEXAS TECH UNIVERSITY
PO BOX 5404 NORTH COLLEGE STATION
ATTN TRAVIS L. SIMPSON
LUBBOCK, TX 79417

TRW DEFENSE & SPACE SYSTEMS GROUP
ATTN TECH INFO CENTER/X-1930
ATTN O. E. ADAMS, R1-1144
ATTN R. K. PLEBUCH, R1-2078
ATTN H. H. HOLLOWAY, R1-2036
ONE SPACE PARK
REDONDO BEACH, CA 90278

TRW DEFENSE & SPACE SYSTEMS GROUP
SAN BERNARDINO OPERATIONS
PO BOX 1310
ATTN EARL W. ALLEN
ATTN F. B. FAY, 527/710
ATTN R. KITTER
SAN BERNARDINO, CA 92402

UNITED TECHNOLOGIES CORP
HAMILTON STANDARD DIVISION
ATTN RAYMOND G. GIGUERE
BRADLEY INTERNATIONAL AIRPORT
WINDSOR LOCKS, CT 06069

VOIGHT CORP
PO BOX 225907
ATTN TECHNICAL DATA CTR
DALLAS, TX 75265

WESTINGHOUSE ELECTRIC CORP
DEFENSE & ELECTRONIC SYSTEMS
CENTER
PO BOX 1693
ATTN HENRY P. KALAPACA, MS 3525
FRIENDSHIP INTERNATIONAL AIRPORT
BALTIMORE, MD 21203

JEAN-MARIE CHARLOT
B.P. 561
92542 MONTROUGE
FRANCE

J. ROTURIER
UNIVERSITE DE BORDEAUX
CENTRE D' ETUDES NUCLEAIRES
LE HAUT-VIGNEAU
33170 GRADIGNAM
FRANCE

DR. L. TOMMASINO
LAB DOSIMETRIA
CNEN-CENTRO STUDI NUCLEARI CASSACCIR
CP 2400-00100
ROME, ITALY

D. BRAUNIG
HAHN-MEITNER-INSTITUT
GLIENICKER STRASSE 100
1000 BERLIN 39 (WANNSU)
FEDERAL REPUBLIC OF GERMANY

HORST P. BRUEMMER
GOSSWINSTR. 14
8000 MUNICH 60
FEDERAL REPUBLIC OF GERMANY

JACQUES A. BERRY
ONERA/CERT
2 AV. ED BELIN
31055 TOULOUSE
FRANCE

MICHEL VIE
CENTRE D'ETUDES
46500 GRAMAT FRANCE

US ARMY ELECTRONICS RESEARCH
& DEVELOPMENT COMMAND
ATTN TECHNICAL DIRECTOR, DRDEL-CT

HARRY DIAMOND LABORATORIES
ATTN CO/TD/TSO/DIVISION DIRECTORS
ATTN RECORD COPY, 81200
ATTN HDL LIBRARY, 81100 (2 COPIES)
ATTN HDL LIBRARY, 81100 (WOODBRIDGE)
ATTN TECHNICAL REPORTS BRANCH, 81300
ATTN LEGAL OFFICE, 97000
ATTN CHAIRMAN, EDITORIAL COMMITTEE
ATTN MORRISON, R., 13500 (GIDEP)
ATTN CHIEF, 21000
ATTN CHIEF, 21100
ATTN CHIEF, 21200
ATTN CHIEF, 21300
ATTN CHIEF, 21400
ATTN CHIEF, 21500
ATTN CHIEF, 22000
ATTN CHIEF, 22100
ATTN CHIEF, 22300
ATTN CHIEF, 22800
ATTN CHIEF, 22900
ATTN CHIEF, 20240
ATTN MCGARRITY, J. M., 22300
ATTN MILETTA, J. R., 21100
ATTN BOESCH, JR., H. E., 22300
ATTN MCLEAN, F. B., 22300
ATTN WINOKUR, P. S., 22300
ATTN BRANDT, H. E., 22300
ATTN MEYER, O. L., 22800
ATTN GILBERT, R. M., 22300
ATTN TRIMMER P., 22100
ATTN VAULT, W., 22100
ATTN EISEN, H., 22800
ATTN WILKIN, N., 22800
ATTN OLDHAM, T. R., 22300 (20 COPIES)